Catena 263 (2026) 109769

Contents lists available at ScienceDirect

Catena

journal homepage: www.elsevier.com/locate/catena

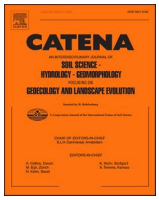

# Hillslope-induced environmental gradients regulate potential soil respiration in temperate peatlands

Yanfei Li [a], Pengzhi Zhao [a,*], Maud Henrion [b], Patrick Gerin [c], Matthieu Leclercq [a], Angus Moore [a], Eléonore du bois d'Aische [b,e], Sébastien Lambot [b], Sophie Opfergelt [b], Veerle Vanacker [a,d], François Jonard [e,1], Kristof Van Oost [a,1]

[a] Earth and Life Institute-Earth & Climate, Université catholique de Louvain, 1348 Louvain-la-Neuve, Belgium
[b] Earth and Life Institute-Environmental Sciences, Université catholique de Louvain, 1348 Louvain-la-Neuve, Belgium
[c] Earth and Life Institute-Applied Microbiology, Université catholique de Louvain, 1348 Louvain-la-Neuve, Belgium
[d] Soil Geography and Landscape Group, Wageningen University, Droevendaalsesteeg 4, Wageningen 6700 AA, The Netherlands
[e] Earth Observation and Ecosystem Modelling Laboratory, SPHERES Research Unit, Université de Liège, 4000 Liège, Belgium

ARTICLE INFO

*Keywords:*
Peat SOM composition
Carbon dynamics
Potential soil respiration
Temperature sensitivity
Northern peatland
Global warming

ABSTRACT

Along peatland catenas, micro- to meso-scale topographic variation shapes microclimate and biogeochemical properties, creating distinct environmental regimes. Yet, how such heterogeneity regulates soil respiration in peatlands has been much less studied. To this end, we sampled five slope positions along a peatland hillslope and combined microclimate monitoring with laboratory incubations and geochemical analyses. Specifically, we asked: (1) How do hillslope-induced environmental gradients influence spatial patterns of potential soil respiration (PSR) in temperate peatlands? and (2) How does PSR respond to increasing temperature? Results showed that soil biogeochemistry (i.e., soil pH, C/N ratio, soil organic matter (SOM) functional groups), PSR rates, and apparent temperature sensitivity (i.e., activation energy, *Ea*) varied substantially across hillslope positions and soil depths. We found that topographical and thermal-hydrological conditions are associated to soil biogeochemistry patterns across the landscape. The spatial heterogeneity in PSR and *Ea* was primarily explained by the functional group composition of SOM (45–68 % and 34 % in total, respectively), with cellulose and carboxylic acids accounting for 27 %–31 % of the variation in PSR rates, while aliphatic and lignin functional groups explained 13 % of the variation in *Ea*. In addition, the C/N ratio and pH together accounted for 13 %–26 % of PSR rate variation and 18 % of variation in *Ea*. This study demonstrates that hillslope topography-driven variations in soil biogeochemical properties strongly regulate potential peat soil respiration and its temperature sensitivity, providing mechanistic insights into peatland carbon–climate feedback and informing peatland management strategies.

## 1. Introduction

Peatlands are globally distributed, with a great majority located between ~45°N-70°N (Loisel et al., 2017). They are known for storing a large amount of carbon, which was estimated at 942.09 ± 312 Gt (Widyastuti et al., 2025). Currently, peatlands are facing elevated threats from both climate change (e.g., warming, drought) and human activities (e.g., drainage, land use change) (Fenner and Freeman, 2011; Hopple et al., 2020; Loisel et al., 2021). For instance, warming and associated changes in hydrology can enhance their carbon emission by increasing oxygen diffusion and shifting vegetation cover (Ofiti et al., 2023; Schuur et al., 2015). As a consequence, peatlands may convert from carbon sinks to carbon sources, releasing substantial amounts of greenhouse gases into the atmosphere (Dorrepaal et al., 2009; Elberling et al., 2013), which in turn causes a positive feedback loop to climate change. At the same time, drainage for agriculture or forestry oxygenates the peat matrix, accelerating aerobic decomposition and further degrading these critical carbon stores (Birnbaum et al., 2023; Sloan et al., 2018; van Giersbergen et al., 2024). Recent studies have reported that degraded peatlands are estimated to emit 2.00 Gt $CO_2$ of

* Corresponding author.
*E-mail address:* pengzhi.zhao@uclouvain.be (P. Zhao).
[1] These authors are co-last authors.

https://doi.org/10.1016/j.catena.2025.109769
Received 24 August 2025; Received in revised form 3 December 2025; Accepted 23 December 2025
Available online 30 December 2025

greenhouse gas emissions annually, accounting for about 4 % of total global emissions resulting from anthropogenic impacts (UNEP, 2022). If such emissions persist, they could consume up to 41 % of the remaining global budget needed to limit warming to below 1.50 °C (UNEP, 2022). Therefore, elucidating the key mechanisms that govern soil respiration in peatlands is crucial for assessing their future fate under global change.

Previous studies have examined how temperature (Treat et al., 2014); water table depth (Berglund and Berglund, 2011); soil pH (Zhang et al., 2020); microbial community (Preston and and Basiliko, 2016); aerobic and anaerobic conditions (Moore and Dalva, 1997), and soil organic matter (SOM) biogeochemical composition (Sjögersten et al., 2016) influence soil organic carbon (SOC) decomposition in northern peatlands. Among these controls, SOM biogeochemical composition has been shown to strongly regulate soil respiration potential: the labile components (e.g., cellulose, glucose) undergo faster consumption due to low metabolic energy barriers, whereas recalcitrant functional groups (e.g., phenolic, aliphatic, lignin) resist microbial decomposition because of their high bond dissociation energies (Leifeld et al., 2012; Normand et al., 2021; Wickland and Neff, 2008). Although these studies have generated valuable insights, they often focus on single factors in isolation. In reality, peatland soil respiration is affected by the combination of multiple interacting environmental drivers, which vary across space due to heterogeneous topography, vegetation, and thermal-hydrological gradients. At the profile scale, water table fluctuations regulate oxygen availability, thereby shaping microbial communities, enzyme activity, and oxidative breakdown of SOC (Fenner and Freeman, 2011). Systematic changes in oxygen supply and microbial activity lead to vertical shifts in SOM chemical composition: labile carbon is preferentially consumed by microorganisms, resulting in a higher proportion of more recalcitrant materials with increasing peat depth (Keiser et al., 2024; Webster et al., 2014). This selective decomposition process also leads to the depletion of nitrogen with depth, resulting in different carbon-to-nitrogen (C/N) ratios at depth that can shift the microbial community's composition and function, ultimately affecting soil respiration traits (Alster et al., 2018; Yu et al., 2022). Consequently, surface and deep peat exhibit distinct soil respiration rates (Li et al., 2021; Normand et al., 2021) and temperature sensitivity (i.e., the degree to which soil respiration increases with rising temperature). (Micro)topography, such as hollows and hummocks, controls the spatial distribution of soil water content, nutrients, vegetation, and thus carbon storage and release even at small scales (Li et al., 2025; Sullivan et al., 2008; Wang et al., 2023; Wang et al., 2021; Winter, 1988). For instance, relatively dry hummocks provide more favorable aerobic conditions that support vascular plants' growth and stimulate microbial activity, thereby accelerating the decomposition of SOM and forming localized $CO_2$ emission hotspots (Becker et al., 2008; Iseas et al., 2024). In contrast, depressions (e.g., hollows) favor the accumulation of water and the growth of *Sphagnum* moss, which produces higher concentrations of uronic acids and decay-resistant litter input to peat soils (Rydin et al., 2006).

In sloping peatlands with a hummocky surface (Winter, 1988), topography-controlled processes further regulate the spatial (re)distribution of water, energy, and nutrients across the landscape (Burt and Pinay, 2005; Glatzel et al., 2024; Holden, 2009; Li et al., 2018), thereby increasing the spatial heterogeneity in SOC pool vulnerability and soil $CO_2$ emission, relative to no-sloping peatlands. More specifically, these topographic gradients create heterogeneity in hydrological regimes (Holden, 2005; Millar et al., 2018; Winter, 1988), dissolved organic carbon (Boothroyd et al., 2015), nitrogen limitation and pH (Philben et al., 2020), microbial biomass ratios (Xu et al., 2022), peat soil thickness (Li et al., 2024), and vegetation composition (Andersen et al., 2011). For example, Glatzel et al. (2024) found that raised bogs retained most of their cellulose by 1 m depth, whereas blanket bogs showed rapid SOM transformation and lost 92 % of cellulose material. Hence, studying spatial heterogeneity provides an opportunity to improve our understanding of the long-term interactions among multiple environmental variables and how they collectively control soil respiration rates and their vulnerability to rising temperatures across multiple spatial scales.

While much progress has been made in understanding carbon dynamics in mineral soils through studies on hillslope effects (e.g., Doetterl et al. (2012); Wiaux et al. (2014); Zhao et al. (2021)), much less is known about the potential carbon loss of peat soils under the long-term influence of hillslope processes. For instance, some studies (e.g., Boothroyd et al. (2015); Wang et al. (2023)) have examined the spatial variation of dissolved organic carbon in peatland pore water. Additionally, Philben et al. (2020) observed higher carbon emission rates under anaerobic conditions at the low-lying toeslope compared to the plateau at the top of the hillslope, which was attributed to a higher concentration of labile carbon, elevated pH, and greater nitrogen availability resulting from erosion, selective leaching, and weathering. These observations suggest that slope position, hydrological conditions, and biogeochemical processes could play an important role in determining carbon emissions, highlighting the need for a more comprehensive understanding of the complex dynamics across the landscape.

To better understand the mechanisms driving carbon loss from these ecosystems, we conducted laboratory incubations using peat samples collected along a temperate peatland hillslope, which is located at the Belgian Hautes Fagnes, the southern margin of the northern peatlands zone in Europe (Loisel et al., 2017). This region is a critical area for assessing potential carbon losses and the vulnerability of European peatland carbon stocks under changing climate conditions and rising anthropogenic pressures. In this study, we aim to address two questions: (1) How do hillslope-induced environmental gradients influence spatial patterns of potential soil respiration (PSR) in temperate peatlands? (2) How does potential soil respiration respond to changes in temperature? To this end, we first characterized the spatial patterns of environmental gradients, PSR rates, and their temperature sensitivity in surface and deep peat across the slope positions. Second, we identified the factors (i.e., SOM biogeochemical composition, soil C/N ratio, soil pH, soil temperature, soil moisture) that are related to spatial variations in PSR. Third, we quantified the contributions of these factors and explored their interactions to understand how they collectively shape the spatial variability in PSR.

## 2. Materials and methods

### 2.1. Study site

The Belgian Hautes Fagnes plateau is situated in eastern Belgium (Fig. 1a), with the highest point reaching 694 m in orthometric elevation (Goemaere et al., 2016). Due to the relatively high altitude, the plateau intercepts clouds and moist vapor from the Atlantic Ocean, resulting in a humid climate. According to meteorological records from 1971 to 2000, the mean annual air temperature in this region was around 6.70 °C, with a mean annual precipitation of about 1439 mm (Mormal and Tricot, 2004). The peatlands in the Belgian Hautes Fagnes cover an area of approximately 3750 ha, which have been formed since the Late Pleistocene and grown under both oceanic and continental influences (Frankard et al., 1998). Large amounts of partly decomposed plant debris initially accumulated in depressions to form peat, which subsequently expanded laterally (Frankard et al., 1998). The vegetation remnants accumulated in the peat record spans a shift from tundra during the Bölling (ca. 13,700–12,400 cal BC) and Dryas III (ca. 10,100–9400 cal BC), to taiga (*Pinus sylvestris*) in the Alleröd and Dryas III, followed by mixed temperate forests (e.g., *Corylus*, *Quercus*, *Ulmus*, *Tilia*, *Alnus–Fraxinus*, *Fagus*) from the Boreal onward (Frankard et al., 1998). It was found that peats accumulated rapidly through the Atlantic, Subboreal, and Subatlantic periods due to the growth of peat mosses (Frankard et al., 1998). Heathlands and grasslands dominated the area from ~800 years ago until the beginning of the 19th century as a result of ancient land use practices (e.g., extensive grazing, peat extraction, harvesting mulch for the stables, cultivation, and tree cutting) (Frankard et al., 1998). From the late 19th to the early 20th century, large-scale

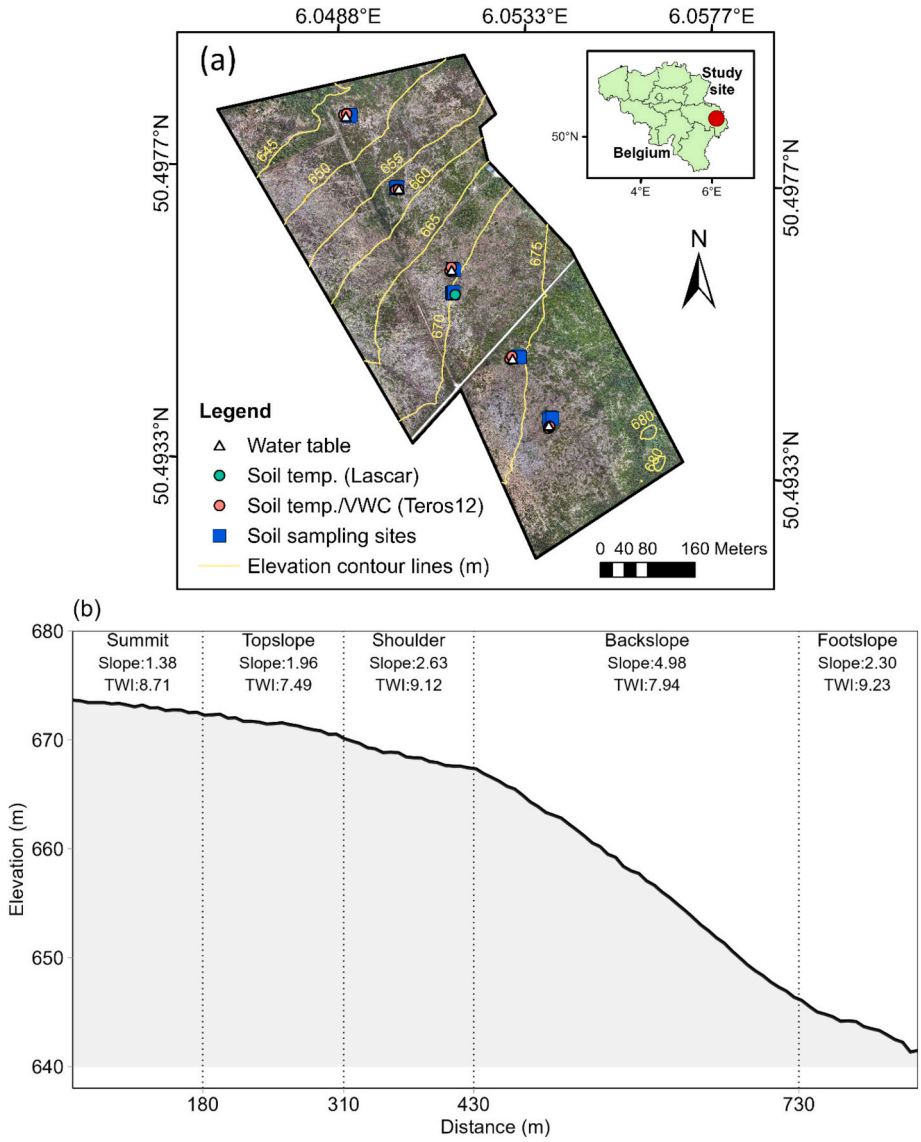


**Fig. 1.** Study site (a) and the elevation profile of the middle transect along the hillslope (b). The coordinate system used is WGS 84 UTM 32 N, with elevations referenced to the ellipsoidal height. Slope indicates the mean slope gradient (°) and TWI indicates the mean terrain wetness index (dimensionless, see our previous work (Li et al., 2024) for the calculation) of sampling sites at each slope position.

plantations of spruce (*Picea abies*) started, accompanied by the excavation of an extensive drainage network to facilitate tree growth (Frankard et al., 1998). Human activities and later invasion of *Molinia caerulea* have heavily impacted the impact of the peatbogs, leading to peat degradation and partial loss of typical peat-forming communities such as *Sphagnum* (Frankard et al., 1998).

Our study site (50.4948 N, 6.0520 E) is a peatland (bog) hillslope with an area of 33 ha, located in the upper valley of the Hoëgne River (Fig. 1a). This ombrotrophic bog is mainly fed by precipitation and characterized by distinct SE-NW-oriented topographic units (i.e., summit, topslope, convex shoulder, backslope, and footslope). The southern part of the hillslope is a plateau, with elevations ranging from 675 m to 680 m, and clear transition toward the topslope and shoulder positions (Fig. 1b). The backslope, which faces toward the north, is steeper than the before-mentioned units with an average slope gradient of 4.98°, and elevations between 645 m and 670 m. The footslope is located at the northern end of the transect, adjacent to the Hoëgne River. The peat thickness ranges from 0.20 to 2.10 m, with deeper peat in the footslope and shallower peat at the topslope positions (Henrion et al., 2024). The SOC stock within the top one-meter layer ranges from 176.13 t $ha^{-1}$ to 856.57 t $ha^{-1}$, with higher values observed at the summit, shoulder, and footslope locations (Li et al., 2024). Due to the heterogeneous characteristics of the landscape, including great spatial variability in soil moisture (Henrion et al., 2025) and soil temperature, the estimated soil respiration exhibited strong spatial variations across the hillslope (Li et al., 2025). The entire hillslope was drained for forestry and planted with spruce (*Picea abies*) in 1914 and 1918, leading to the construction of numerous drainage ditches (with a total number of ~40 observable big channels, from our drone-derived Digital Terrain Model (Li et al., 2024)). Trees were progressively cleared between 2000 and 2016. Since 2017, the site has been under restoration, and now covered by *Vaccinium myrtillus*, *Molinia caerulea*, *Juncus acutus*, and various peat moss species, besides a few hardwood species (e.g., *Betula pubescens* and *Quercus robur*) (Li et al., 2024).

### 2.2. Soil sampling

In August 2024, a total of 17 soil profiles were excavated to a depth of 80 cm along five slope positions of the hillslope transect (Fig. 1). For summit, topslope, backslope, and footslope positions, three sites

previously used for in-situ soil respiration measurements (Li et al., 2025) were selected and spaced 1-5 m apart, yielding 12 (4 × 3) profiles. At the shoulder position where soil water content is highly variable (Henrion et al., 2025), three profiles were sampled in a drier area (i.e., shoulder dry) and two profiles in a wetter area (i.e., shoulder wet), yielding 5 profiles. At each profile, soil samples were taken at two depths (i.e., 10–20 cm and 60–70 cm), resulting in a total of 34 samples for analysis. In parallel, 34 undisturbed samples were taken with a 100 $cm^3$ Kopecky ring for the determination of soil bulk density. All the samples were placed in an insulation box immediately after collection. They were then transported to the laboratory freezer and stored at −20 °C until analysis.

### 2.3. Soil temperature, moisture, and water table monitoring

We monitored the temporal evolution of soil temperature (°C) and volumetric water content (VWC, $cm^3\ cm^{-3}$) near the soil sampling sites using Teros12 sensors (Meter Group, München, Germany), deploying two replicates per slope position at 5 m spacing (Fig. 1a; Henrion et al. (2025)). These sensors recorded data at 10 cm and variable deeper depths (ranging from 50 cm to 90 cm, depending on peat depth and composition) from October 2022 to October 2024, every 10 min. In addition, five Levelogger 5 pressure sensors (Solinst, Georgetown, Canada) were placed in PVC pipes along the main transect adjacent to the soil sampling locations to capture pressure, which was then used to interpret groundwater dynamics (Henrion et al., 2025). These units also recorded at 10-min intervals, from May 2023 through September 2024. At the shoulder slope positions, we first installed Teros12 and water level sensors in the wetter areas, while in drier areas, we only installed a soil temperature sensor (EL-USB-1-PRO, Lascar, United Kingdom), which recorded data from March 2023 to October 2024. Given variations in the duration of monitoring, our analysis focuses on the period between 1 June 2023 and 31 May 2024 when all data —soil temperature, volumetric water content, and water-table depth—are available. Finally, drone-borne ground-penetrating radar was used to map soil moisture to a depth of 40 cm, over a full year and 19 different dates, highlighting spatial patterns and their dynamics across the full test site (Henrion et al., 2025).

### 2.4. Laboratory soil analysis

The undisturbed soil samples were oven-dried at 105 °C for 48 h to a constant mass. Soil bulk density (BD, g $cm^{-3}$) was then determined by dividing the dry mass by the original sample volume. The gravimetric water content (GWC, g $g^{-1}$) was calculated by dividing the mass of water lost after oven-drying by the mass of the oven-dry soil. Total soil porosity was calculated from bulk density and particle density, assuming a particle density of 1.4 g $cm^{-3}$ for peat samples (Lal and Shukla, 2004) and 2.65 g $cm^{-3}$ for mineral soil samples (Skopp, 2000). The soil VWC of each sample was then determined by multiplying GWC by the soil BD. A subset of disturbed soil samples was oven-dried at 80 °C for 24–48 h, then crushed and ground into a fine powder. The presence of inorganic carbon in each sample was tested by adding a drop of 10 % HCl, but no reaction was observed, indicating the absence of a significant amount of inorganic carbon. As such, soil organic carbon (SOC, %) and total nitrogen (TN, %) contents were determined using ~0.3 g of each homogenized subsample, which were heated at 1100 °C in the analyzer (928 Series, LECO analyzer, United States). A subset of dried samples was wetted with deionized water for soil pH measurement. Approximately 5 g of each homogenized subsample was placed into a centrifuge tube and mixed with about 25 milliliters of deionized water. The tubes were then shaken for 2 h to fully blend the soil and water, after which soil pH was measured using a pH Meter (FiveEasy pH/mv Instruments, METER TOLEDO, Switzerland).

All ground soil samples with two replicates were scanned in the laboratory using a compact Fourier-Transform Infrared Spectrometer (ALPHA II, Bruker, United States) in the mid-infrared (MIR) range (400–4000 $cm^{-1}$) with a spectral resolution of 2 $cm^{-1}$. We then followed the method described in Artz et al. (2008) and Webster et al. (2014) to semi-quantitatively calculate the relative abundance of eight SOM functional groups (Table 1). First, each absorbance spectrum was normalized by subtracting its minimum value and then dividing its mean value over its wavenumber range. We then calculated the height (from the normalized minimum set at 0) of the absorbance peak at the wavenumber set for each functional group, which was used to represent its relative abundance (Absorbance *normalized_peak* / Mean_Absorbance *normalized_spectrum*). The description and corresponding wavenumber of each functional group is summarized in Table 1.

### 2.5. Potential soil respiration measurements

Our incubation design intentionally isolated temperature effects; thus, we kept the moisture content of the sample fixed to avoid a direct effect of soil water content. For our purpose, a subset of disturbed wet soil samples was used for soil incubation experiments. In order to minimize the effects of freezing the samples, we gradually thawed and pretreated the samples. After thawing the sample at 40 °C for around 12 h, we manually removed visible plant roots to minimize their influence on potential $CO_2$ production (Dioumaeva et al., 2002). A portion of these pretreated samples was then used to determine soil VWC, which provided the basis for adjusting all samples to a standardized moisture condition. Each sample was subsequently adjusted to a uniform moisture content of 0.70 $cm^3\ cm^{-3}$, which is close to the observed annual mean field VWC of 0.78 ± 0.17 $cm^3\ cm^{-3}$ across the hillslope, by placing over-wet samples in a ventilated room or adding deionized water to over-dry samples until the targeted *V*WC was reached. The incubation experiments were then conducted at three temperatures (i.e., 5 °C, 15 °C, and 25 °C). The 5 °C and 15 °C were chosen to represent the range of daily mean temperatures of all sites during winter (range: 3.96–7.77 °C; mean ± SD: 5.32 ± 1.01 °C) and summer (range: 9.77–15.04 °C; mean ± SD: 12.73 ± 1.45 °C), respectively, based on measurements from October 2022 and October 2024. The 25 °C treatment was included to simulate a potential extreme warming scenario. Each soil sample was incubated with three replicates. In addition, we classified all samples ($n$ = 34) into peat soil and mineral soil based on their SOC content (Dettmann et al., 2021). Only the peat samples (SOC

**Table 1**
Descriptions and corresponding wavenumbers of absorbance peaks assigned to the SOM biogeochemical composition. N.A. indicates data that was not available.

| SOM biogeochemical composition | Description | Wavenumber $cm^{-1}$ | | |
|---|---|---|---|---|
| | | Artz et al. (2008) | Webster et al. (2014) | This study |
| Lignin backbone | C–O stretching of phenolic OH, arylmethylethers | 1265 | 1262 | 1274 |
| Phenolic 1382 | Phenolic (lignin) and aliphatic structures | 1371 | 1382 | 1382 |
| Carboxylate | Carboxylate/carboxylic structures | 1426 | 1414 | 1426 |
| Phenolic 1458 | Phenolic (lignin) and aliphatic structures | 1450 | 1452 | 1458 |
| Carboxylic acids | Carboxylic acids (-COOH or -COOR structure) | 1720 | N.A. | 1714 |
| Aliphatic 2858 | Symmetric $CH_2$ structure; fats, wax, lipids | 2850 | 2850 | 2858 |
| Aliphatic 2926 | Antisymmetric $CH_2$ structure; fats, wax, lipids | 2920 | 2919 | 2926 |
| Cellulose | O–H stretching of cellulose | 3340 | 3293 | 3378 |

> 16.80 %, $n = 28$) were used in the incubation experiment. For each replicate peat sample, we placed approximately 30–50 g (wet weight, accurately measured) of soil into 500 ml mason jars. Sample volume in the jar was verified by water-displacement: an equal wet mass was placed in a separate jar, the volume of displaced water was measured, and water density was assumed to be 1 g $mL^{-1}$ at 20 °C. A total of 252 jars was prepared and sealed with Parafilm to minimize water loss. They were then placed in three incubators (TC series, Lovibond, U.K.) set to 5 °C, 15 °C, and 25 °C, respectively, for a 10-day climatic acclimation to stabilize microbial activity and minimize $CO_2$ pulses due to sample preparation. The formal incubation experiment began on day 11 and continued for 4 months (i.e., began on 2 October 2024 and ended on 31 January 2025). We note that sample selection and handling (e.g., disturbance, freezing–thawing, root-picking, and subsequent homogenization) may have altered soil structure, porosity, and aeration, thereby influencing microbial respiration, and we acknowledge that this is a limitation of the study. Also, the controlled laboratory conditions of during the incubation experiments cannot fully replicate the complexity of field environments.

During incubation, the mason jars were sealed with metal lids with two valves for at least 24 h before gas sampling. The syringe was first purged three times to remove all residual air and was then connected to the valve of the mason jar. To thoroughly mix the gas inside, the syringe was pushed and pulled three times. Subsequently, approximately 20 ml of mixed gas was then withdrawn using a syringe and the relative abundances of $CO_2$ ($pCO_2$, ppm) and $CH_4$ ($pCH_4$, ppm) were analyzed by gas chromatography with a thermal conductivity detector (GC-TCD, CompactGC 4.0, Interscience B.V., The Netherlands). This gas analyzer was calibrated to quantify the proportions of $H_2$, $O_2$, $N_2$, $CO_2$, $CH_4$, and $H_2O$ present in the gas sample (Henry et al., 2023). No detectable $CH_4$ was found during the entire incubation period. The atmosphere $CO_2$ concentration ($pCO_2ref$, ppm) was also measured as a reference every time before measuring the sample. For the first two months, gas sampling for soils incubated at 5 °C was conducted once per week, while for soils at 15 °C and 25 °C, gas sampling was conducted twice in the first week and once per week thereafter. In the third month, gas sampling took place once every two weeks, and thereafter once every three weeks. Deionized water was added to the samples every month to maintain a constant moisture condition (as measured by total jar mass).

### 2.6. Potential soil respiration assessment

#### 2.6.1. Calculate potential soil respiration rate

First, we calculated the accumulation rate of $CO_2$ in the mason jar, and then calculated the rate of produced $CO_2$-C using the ideal gas law equation:

$$rCO_2C = \frac{pCO_2 - pCO_2ref}{Time} \times \frac{Vgas}{1000000} \times \frac{P}{Rv \times Tincu} \times 12 \quad (1)$$

where $rCO_2C$ is the rate of $CO_2$-C produced (g $CO_2$-C $h^{-1}$); $pCO_2$ is the concentration of accumulated $CO_2$ (ppm) in the mason jar; $pCO_2ref$ is the reference $CO_2$ concentration (ppm) in the air; *Time* indicates the gas accumulation time (hour); *Vgas* indicates the net volume of the headspace of each mason jar, measured by water displacement before the experiment, and taking into account the net volume occupied by the sample (mass of sample / volume mass, assumed to 1 kg $L^{-1}$); *P* is the reference pressure (atm); *Rv* is the gas constant (equal to 0.082057 L atm (mol K)$^{-1}$); *Tincu* is the temperature of the gas in the jar headspace (i.e., the incubation temperature: 5 °C, 15 °C, and 25 °C respectively, convert to unit in K); 12 is the molar mass of carbon. Then, we calculated the potential soil respiration (PSR) rates as the amount of $CO_2$-C produced per unit of SOC over a four-month incubation period using the following formula:

$$PSR\ rate = \left( \sum \frac{rCO_2C \times 1000000}{pSOC \times Gsample} \right) \times \frac{1}{n} \quad (2)$$

where, *PSR rate* is the mean potential soil respiration rate (μg $CO_2$-C g $SOC^{-1}$ $h^{-1}$); *pSOC* is SOC content (g $g^{-1}$); *Gsample* is the dry mass of the incubated soil sample (g); *n* represents the total number of measurements conducted over the four-month incubation period.

#### 2.6.2. Calculate apparent temperature sensitivity

The apparent temperature sensitivity of potential soil respiration was expressed as activation energy ($E_a$; kJ $mol^{-1}$), which was calculated by the Arrhenius equation:

$$E_a = (ln\ A - lnPSR\ rate) \times Rg \times Tincu \times 1000 \quad (3)$$

where, *Tincu* is the incubation temperature (K), *Rg* is the gas constant (equal to 8.314 J (mol K)$^{-1}$), and *A* is the pre-exponential factor.

### 2.7. Statistical analysis

All data analyses were performed in RStudio V4.1.2. Differences among slope positions/depths were assessed using the Kruskal-Wallis test, a non-parametric alternative to the one-way analysis of variance, and suitable for small sample sizes and non-normally distributed data (Dunn, 1964). If the *Kruskal-Wallis* test detected a significant overall effect ($p < 0.05$), post-hoc pairwise comparisons were conducted using *Dunn's* test ($p < 0.05$). Pearson correlation coefficients were calculated to assess relationships between variables (Murdoch and Chow, 1996). Additionally, mixed-effects linear regressions were used to examine the influence of topography on soil biogeochemical properties (i.e., C/N ratio and cellulose), with slope position included as a random effect. The models for identifying factors controlling spatial variations in PSR rates and their temperature sensitivity are introduced below.

Multiple linear regressions were employed to identify factors controlling PSR, with the respiration rates under three incubation temperature treatments and activation energy ($E_a$) as responses, respectively. The regression models are defined as:

$$Response = \beta_0 + \beta_1 x_1 + \beta_2 x_2 + \ldots + \beta_p x_p + \epsilon \quad (4)$$

where, $\beta_0$ indicates the intercept, $\beta_i$ is the regression coefficient of the independent variable $x_i$, and $\epsilon$ indicates the residual error. The input variables included relative abundance of SOM biogeochemical composition (i.e., the relative abundance of cellulose, lignin backbone, carboxylate, carboxylic acids, phenolics (i.e., 1382 $cm^{-1}$ and 1458 $cm^{-1}$), and aliphatics (i.e., 2858 $cm^{-1}$ and 2926 $cm^{-1}$)), soil C/N ratio, soil pH, soil temperature and VWC.

Given the correlations and co-linearity among different types of SOM biogeochemical composition and their correlation with other variables (Table S1), a Principal Component Analysis (PCA) followed by Varimax rotation was first performed to reduce the data dimension and address multicollinearity (Grice, 2001; Jolliffe, 2002; Revelle, 2009). Rotated components (RCs) with the cumulative explained variance of more than 90 % were retained as predictors for subsequent multiple linear regression to avoid multicollinearity and overfitting (Table S2). The contribution of each variable to the overall explained variance was quantified using the *relaimpo* package (Groemping, 2006). Multicollinearity was assessed by the variance inflation factor (*VIF*; Fox and Monette (1992)) after running each model. Regression model fit was evaluated by the coefficient of determination ($R^2$) and root mean squared error (*RMSE*).

## 3. Results

### 3.1. Thermal-hydrological conditions and soil characteristics

At most sites, topsoil (i.e., 10 cm) daily temperatures were warmer than those of the deep peat layer (i.e., 50–90 cm) from April to October, while in other months, the deep peat was warmer than topsoil (Fig. 2a).

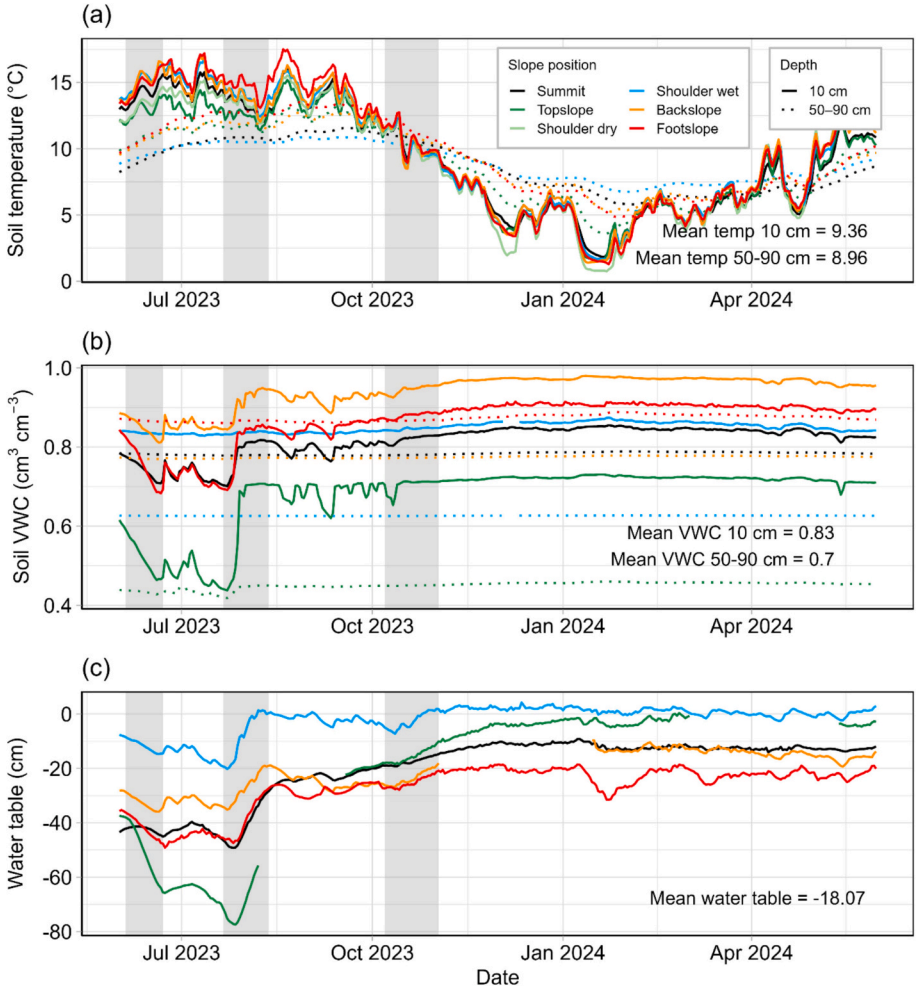


**Fig. 2.** Thermal-hydrological conditions across different slope positions and depths along the hillslope: daily mean soil temperature (a), daily mean soil VWC (b), and daily mean water table (c). Positive values of the water table indicate levels above the peat surface. The grey shading in each subplot indicates the periods (based on 14 days moving window) when the water table and soil VWC at 10 cm depth were significantly correlated across all sites, representing times when water table fluctuations affected surface peat moisture.

In general, topsoil temperatures (e.g., footslope, range: 1.29–17.50 °C; mean ± one standard deviation (SD): 9.72 ± 4.63 °C) showed greater annual fluctuations than deep peat temperatures (e.g., shoulder wet, range: 6.75–10.85 °C; mean ± SD: 8.94 ± 1.37 °C). Soil volumetric water content (VWC) of both topsoil and deep peat exhibited substantial spatial heterogeneity (Fig. 2b). The backslope topsoil had the highest VWC (0.94 ± 0.04 $cm^3$ $cm^{-3}$), wetter than other slope positions and the corresponding deep peat (0.78 ± 0.01 $cm^3$ $cm^{-3}$). In contrast, the

**Table 2**
Dominant modern vegetation cover, soil type, bulk density, SOC, TN, C/N ratio, pH, and total soil porosity in the soil sample before incubation at different slope positions. Values are presented as mean ± one standard deviation (SD). The *Kruskal-Wallis* and *Dunn's test* was conducted to determine if there were significant differences among slope positions and sampling depths, with different letters indicating significant differences ($p < 0.05$). The numbers in the bracket indicate the sample size.

| Slope position | | Summit | Topslope | Shoulder dry | Shoulder wet | Backslope | Footslope |
|---|---|---|---|---|---|---|---|
| Vegetation | | *Molinia caerulea* | *Vaccinium myrtillus* | *Molinia caerulea* | *Juncus acutus* | *Vaccinium myrtillus* | *Molinia caerulea* |
| Soil type | 10–20 cm | peat | peat | peat | peat | peat | peat |
| | 60–70 cm | mineral | mineral | peat | peat | peat | peat |
| Bulk density ($g\ cm^{-3}$) | 10–20 cm | $0.22 \pm 0.03^{abc}$ | $0.36 \pm 0.03^{ab}$ | $0.19 \pm 0.01^{abcd}$ | $0.16 \pm 0.01^{cd}$ | $0.19 \pm 0.02^{abcd}$ | $0.17 \pm 0.006^{bcd}$ |
| | 60–70 cm | $1.27 \pm 0.03^{a}$ | $1.34 \pm 0.18^{a}$ | $0.17 \pm 0.08^{cd}$ | $0.13 \pm 0.01^{d}$ | $0.15 \pm 0.02^{cd}$ | $0.14 \pm 0.004^{cd}$ |
| SOC (%) | 10–20 cm | $48.02 \pm 2.39^{ab}$ | $32.58 \pm 5.33^{b}$ | $52.23 \pm 0.68^{a}$ | $51.43 \pm 3.15^{a}$ | $39.97 \pm 0.46^{ab}$ | $32.37 \pm 2.16^{b}$ |
| | 60–70 cm | $2.73 \pm 0.53^{c}$ | $1.11 \pm 0.20^{c}$ | $44.72 \pm 7.15^{ab}$ | $41.45 \pm 7.64^{abc}$ | $44.45 \pm 4.24^{ab}$ | $48.33 \pm 1.90^{ab}$ |
| TN (%) | 10–20 cm | $1.92 \pm 0.15^{abc}$ | $1.39 \pm 0.35^{bcd}$ | $2.32 \pm 0.10^{ab}$ | $2.34 \pm 0.28^{abc}$ | $2.54 \pm 0.19^{a}$ | $1.77 \pm 0.12^{abcd}$ |
| | 60–70 cm | $0.08 \pm 0.01^{d}$ | $0.07 \pm 0.01^{d}$ | $2.29 \pm 0.40^{abc}$ | $1.62 \pm 0.27^{abcd}$ | $1.40 \pm 0.36^{bcd}$ | $1.36 \pm 0.17^{cd}$ |
| C/N ratio | 10–20 cm | $25.12 \pm 2.46^{ab}$ | $23.75 \pm 2.08^{ab}$ | $22.56 \pm 1.15^{abc}$ | $22.27 \pm 4.05^{abc}$ | $15.79 \pm 1.01^{c}$ | $18.27 \pm 0.96^{bc}$ |
| | 60–70 cm | $35.47 \pm 2.72^{a}$ | $18.37 \pm 0.62^{bc}$ | $19.57 \pm 0.63^{bc}$ | $25.55 \pm 0.48^{ab}$ | $32.73 \pm 5.03^{a}$ | $35.87 \pm 5.20^{a}$ |
| Soil pH | 10–20 cm | $3.73 \pm 0.10^{c}$ | $3.93 \pm 0.17^{bc}$ | $3.96 \pm 0.04^{bc}$ | $3.90 \pm 0.15^{bc}$ | $3.73 \pm 0.10^{c}$ | $3.80 \pm 0.08^{c}$ |
| | 60–70 cm | $4.87 \pm 0.09^{a}$ | $4.40 \pm 0.10^{ab}$ | $4.02 \pm 0.04^{abc}$ | $3.85 \pm 0.11^{bc}$ | $4.41 \pm 0.15^{ab}$ | $4.40 \pm 0.10^{ab}$ |
| Total soil porosity ($cm^3\ cm^{-3}$) | 10–20 cm | $0.84 \pm 0.02^{bcd}$ | $0.74 \pm 0.02^{cd}$ | $0.86 \pm 0.01^{abcd}$ | $0.89 \pm 0.01^{abc}$ | $0.87 \pm 0.02^{abcd}$ | $0.88 \pm 0.004^{abc}$ |
| | 60–70 cm | $0.52 \pm 0.01^{d}$ | $0.49 \pm 0.07^{d}$ | $0.88 \pm 0.06^{ab}$ | $0.91 \pm 0.001^{a}$ | $0.89 \pm 0.01^{ab}$ | $0.90 \pm 0.003^{ab}$ |

topslope was relatively dry, with annual mean VWC values of 0.68 ± 0.08 $cm^3$ $cm^{-3}$ for top layers and 0.45 ± 0.04 $cm^3$ $cm^{-3}$ for deep layers (i.e., mineral soil, saturated or near saturation). Furthermore, the water table at the topslope showed large fluctuations throughout the year (range: −77.44-0.35 cm; mean ± SD: −21.63 ± 25.17 cm), as shown in Fig. 2c. At the shoulder wet slope position, however, the water table remained close to the surface and relatively stable within one year (range: −20.22-4.21 cm; mean ± SD: −2.15 ± 5.62 cm).

Across the hillslope, peat soils were consistently observed at the surface (i.e., 10–20 cm) at all slope positions (Table 2). In contrast, mineral soil was only found in the deep layer (i.e., 60–70 cm) at the summit and topslope positions, characterized by high bulk density and low SOC content (Table 2). For the purpose of this study, the following results and discussion will focus on the peat soils; characteristics of mineral soils are not shown hereafter. Topsoil SOC content at the footslope (32.37 ± 2.16 %) and topslope (32.58 ± 5.33 %) was lower than at the shoulder positions, both dry (52.23 ± 0.68 %) and wet (51.43 ± 3.15 %). The TN content in the topsoil was higher at the backslope than at the topslope, despite a similar modern dwarf shrub vegetation covering at both locations (Table 2). However, the SOC and TN content in the deep peat showed no pronounced spatial variation across the landscape. The topsoil C/N ratio was higher at the summit compared to the backslope, whereas the C/N ratio of deep peat was higher at the footslope (Table 2). Topsoil pH also showed spatial heterogeneity along the hillslope despite the small range, with the summit and backslope being more acidic than other slope positions (Table 2). In contrast, for the deep peat layer, the shoulder position had lower pH than at the footslope and backslope (Table 2). In general, pH values of deep peat

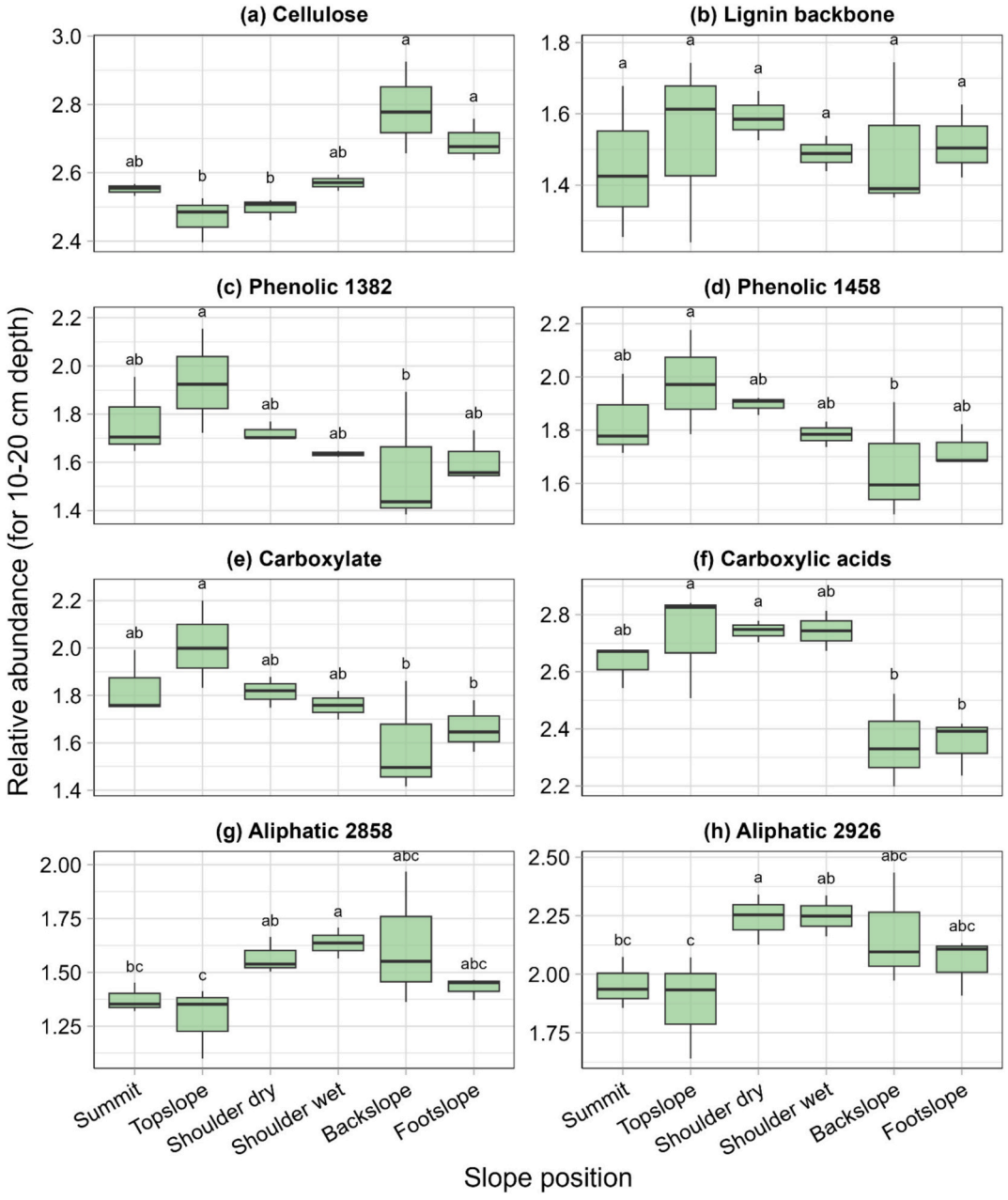


**Fig. 3.** Relative abundance of functional groups at different slope positions and a depth of 10–20 cm ($n = 17$). The lower and upper edges of each box represent the first and third quartiles, respectively, while the line inside the box indicates the median. The whiskers extend to the smallest and largest values that fall within 1.5 times the interquartile range from the lower and upper quartiles. The *Kruskal-Wallis* and *Dunn's test* was conducted to determine if there were significant differences among slope positions for a given depth, with different letters indicating significant differences.

were higher than those measured at the top layer at most sites, and peat had lower pH values compared to mineral soils (Table 2). The total porosity of the surface layer at the toplsope (0.74 ± 0.02 $cm^3$ $cm^{-3}$) was lower than at shoulder wet, backslope, and footslope positions (Table 2). While for deep samples, mineral soil samples at the summit and topslope had lower porosity compared to peat (Table 2).

### 3.2. Peat SOM biogeochemical composition

Using the Fourier-Transform Infrared Spectrometer in the mid-infrared region, we identified and semi-quantified multiple functional groups in peat SOM, including cellulose, carboxylic acids, phenolics, carboxylate, aliphatic, and lignin (Table 1). The relative abundance of functional groups at two depths and Pearson correlations with C/N ratio and pH are summarized in Table S1. Peat SOM biogeochemical composition displayed substantial spatial variation along the hillslope (Fig. 3, Fig. S1). The relative abundance of cellulose in the topsoil was higher at the footslope (2.69 ± 0.06) and backslope (2.78 ± 0.13) than at the topslope (2.47 ± 0.07) and shoulder dry (2.50 ± 0.03) locations (Fig. 3a). In contrast, cellulose abundance in the deep peat was lower (2.46 ± 0.01) (Fig. S1a). For the lignin backbone (Fig. 3b), no significant differences were observed in the topsoil among slope positions. However, in the deep peat, the shoulder wet (1.34 ± 0.09) showed lower relative abundance compared to footslope (1.76 ± 0.10) (Fig. S1b). Topsoil phenolics were more abundant at the topslope than at the backslope, while in the deep peat, the shoulder wet had lower phenolic content (Fig. 3c, d). Topsoil carboxylate and carboxylic acids were more abundant at the topslope position, with higher values than the footslope and backslope (Fig. 3e, f). In the deep peat, however, their spatial differences were less pronounced (Fig. S1e, S1f). The aliphatic structures in the topsoil were less abundant at the summit and topslope compared to shoulder slope positions (Fig. 3g, h). Conversely, the deep peat at the footslope and backslope showed higher relative abundances of these aliphatic functional groups (Fig. S1g, S1h).

### 3.3. Correlations between soil biogeochemistry and topographical and thermal-hydrological conditions

As shown in Fig. 4a, peat soil biogeochemical properties were strongly influenced by topographical variables (i.e., elevation, TWI, and slope gradient) and thermal-hydrological conditions (soil temperature and VWC). This pattern is consistent with the well-established influence of site topography on soil moisture distribution, as recently highlighted by Henrion et al. (2025). At 10–20 cm depth, most properties (carboxylic acids, carboxylate, phenolics, and C/N ratio) were positively related to elevation, while cellulose exhibited a strong negative relationship ($r = -0.72$, $p < 0.01$). In contrast, cellulose was positively correlated with TWI ($r = 0.57$, $p < 0.05$), soil VWC ($r = 0.78$, $p < 0.001$), and soil temperature ($r = 0.73$, $p < 0.001$), while most other properties showed negative correlations. Aliphatics in the topsoil were more strongly related to slope (Fig. 4a). At 60–70 cm depth, most properties (except cellulose) were negatively correlated with elevation (particularly C/N ratio, $r = -0.85$, $p < 0.001$), while their correlations with slope and TWI were generally weak. The carboxylic acids, aliphatics, lignin backbone, soil pH, and C/N ratio of deep soil showed significant positive correlations with soil temperature and VWC (Fig. 4a).

Linear mixed-effects model showed that the elevation explained 59 % and 68 % of the variance in the C/N ratio for the topsoil and deep layer, respectively (Fig. 5a). For cellulose, elevation accounted for 48 % of the variance in the topsoil and 16 % in the deep layer (Fig. 5b). When slope gradient or TWI were used as fixed effects, the random effect of slope position explained most of the variance in both the C/N ratio and cellulose across depths (Fig. 5), indicating that topographic position exerted a strong control on peat soil biogeochemical properties. Consistent with correlation analysis, soil temperature and soil VWC had similar contributions to spatial variability of the C/N ratio, explaining 32 % and 29 % of the variance in the topsoil and 66 % and 67 % in the deep layer, respectively (Fig. 6). For cellulose, thermal-hydrological conditions explained a moderate proportion of the variance in the topsoil (i.e., 45 % and 57 %), but only a small proportion in the deep layer (i.e., 17 % and 16 %) (Fig. 6).

### 3.4. Potential soil respiration rate and apparent temperature sensitivity

As expected, PSR rates increased with rising temperature over the entire incubation period, while the PSR rates varied largely with topographic position (Fig. 7a, b). Topsoil PSR rates were higher at the footslope position than at the summit under both 5 °C and 15 °C incubation conditions (Fig. 7a). Under the 25 °C treatments, topsoil PSR rates were lower at the topslope (4.95 ± 1.424 μg $CO_2$-C g $SOC^{-1}$ $h^{-1}$) and summit (5.22 ± 0.57 μg $CO_2$-C g $SOC^{-1}$ $h^{-1}$) locations than footslope (8.08 ± 1.58 μg $CO_2$-C g $SOC^{-1}$ $h^{-1}$). In contrast, for the deep peat layer, PSR rates were slower at the footslope (Fig. 7b). The shoulder dry and wet areas showed consistently faster PSR rates across all temperature treatments. The cumulative proportion of respired SOC over the four months incubation is shown in Fig. S2.

The overall apparent temperature sensitivity, represented by activation energy (*Ea*), also varied with slope positions and soil depth (Fig. 7c). Topsoil *Ea* was higher at the summit (76.49 ± 1.54 KJ $mol^{-1}$) and backslope (76.69 ± 6.34 KJ $mol^{-1}$) positions compared to the topslope positions (67.62 ± 5.35 KJ $mol^{-1}$). In the deep layer, *Ea* was highest at the shoulder dry area (73.90 ± 5.59 KJ $mol^{-1}$).

### 3.5. Correlation analysis and factors controlling potential soil respiration

Pearson correlation analysis showed that PSR rates were strongly related to elevation, but the direction of the relationship differed between depths (Fig. 4b). PSR rates were positively associated with the relative abundance of cellulose (Fig. 4c). In contrast, they were negatively correlated with carboxylic acids, aliphatic, and phenolic functional groups. Similarly, apparent temperature sensitivity (i.e., *Ea*) was negatively correlated with aliphatics (2858 $cm^{-1}$: $r = -0.45$, $p < 0.05$; 2926 $cm^{-1}$: $r = -0.48$, $p < 0.01$), and phenolic at 1458 $cm^{-1}$ ($r = -0.40$, $p < 0.05$). Both the C/N ratio and pH had negative relationships with PSR rate and their apparent temperature sensitivity, whereas neither field peat moisture nor temperature showed significant correlations with either variable (Fig. 4c).

Multiple linear regressions were conducted to identify the factors controlling the spatial heterogeneity of PSR rate and their apparent temperature sensitivity. The first five rotated components (RCs), which explained 95 % of total variance and captured the main variation of the three types of variables (Table S2), were selected as input variables for the multiple regression analysis. As shown in Table 3, the three categories of predictor variables could explain 45 %, 57 %, and 68 % of the spatial variation in PSR rates under incubation temperatures of 5 °C, 15 °C, and 25 °C, respectively. Among them, SOM biogeochemical compositions emerged as key drivers of the spatial variability in PSR rates, accounting for 32 %, 36 %, and 41 % of the explained variance as temperature increased. Specifically, RC2 representing cellulose and carboxylic acids was the most influential factor, explaining 27 %-31 % of the variance. This was followed by RC1, associated with aliphatics and lignin backbone, which accounted for 3 %-9 % of the variance. In contrast, RC3 represented by phenolics and carboxylate functional groups played a comparatively minor role, contributing ≤1 % to the spatial variation in PSR rates. Other soil biogeochemical properties also strongly influenced the PSR rates (Table 3). The contribution of RC4, associated with C/N ratio and pH, increased from 13 % at 5 °C to 26 % at 25 °C. Thermal-hydrological conditions (RC5, soil VWC and temperature), had relatively limited direct effects on PSR rates, accounting for less than 1 % of the explained variance across temperature treatments.

Regarding the apparent temperature sensitivity (*Ea*) of peat respiration, all variables combined explained 36 % of its spatial variability

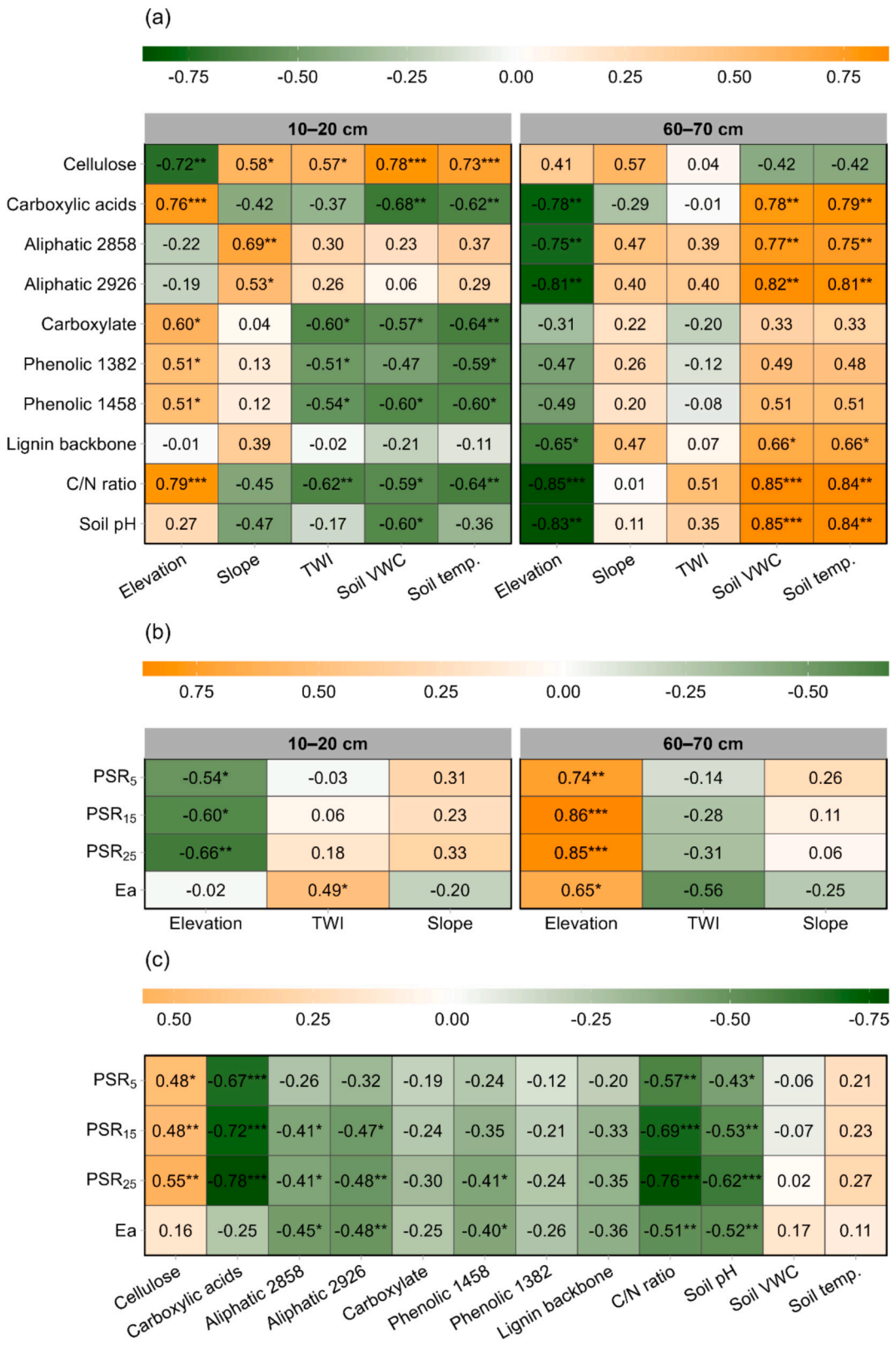


**Fig. 4.** Pearson correlation analysis between (a) soil biogeochemical properties and topographical variables as well as thermal-hydrological conditions at two soil depths (10–20 cm: $n = 17$; 60–70 cm: $n = 11$); (b) potential soil respiration (i.e., PSR rates under three temperature treatments: $PSR_5$, $PSR_{15}$, $PSR_{25}$; and *Ea*) and topographical variables at two soil depths (10–20 cm: $n = 17$; 60–70 cm: $n = 11$); (c) potential soil respiration and SOM biogeochemical composition ($n = 28$), other soil biogeochemical properties (i.e., C/N ratio and pH, $n = 28$), and thermal-hydrological conditions (i.e., mean soil VWC ($n = 10$) and soil temperature ($n = 11$)). Significance level: *** $p < 0.001$, ** $p < 0.01$, * $p < 0.05$.

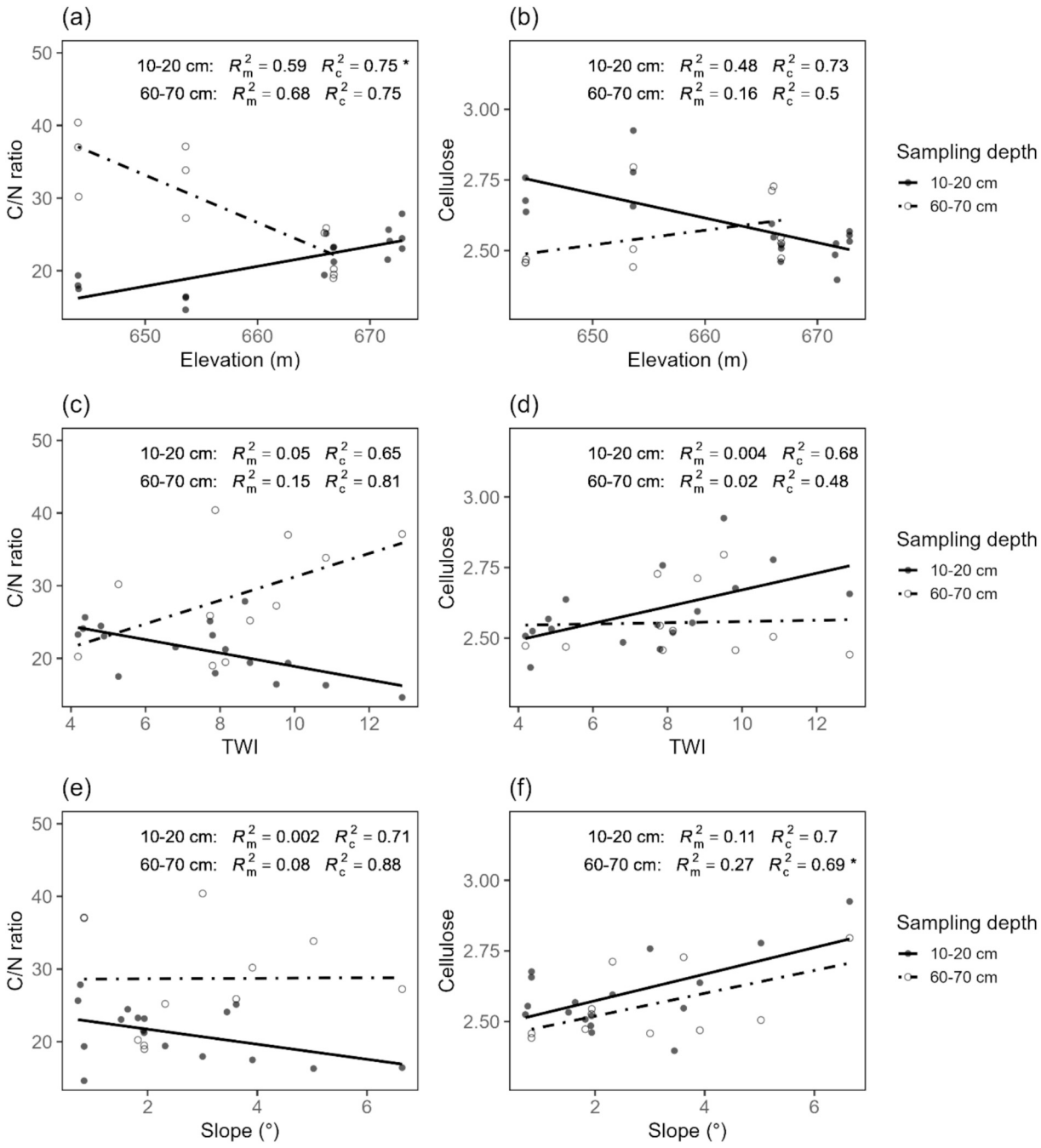


**Fig. 5.** Relationships between C/N ratio and (a) elevation, (c) TWI, and (e) slope, and between the relative abundance of cellulose and (b) elevation, (d) TWI, and (f) slope. Mixed-effects linear regression models were fitted separately for the 10–20 cm and 60–70 cm soil layers, with slope position included as a random effect. The legend reports marginal $R^2$ (*Rm*) and conditional $R^2$ (*Rc*) for each model. Significance level: *** $p < 0.001$, ** $p < 0.01$, * $p < 0.05$.

(Table 3). Specifically, soil C/N ratio and pH (RC4) together could explain 18 % of variance, followed by RC1 (aliphatics and lignin; 13 %). The contributions from RC2 (cellulose and carboxylic acids) and RC3 (phenolics and carboxylate) remained minor (≤ 3 %). The thermal-hydrological conditions (RC5, soil VWC and temperature) together accounted for 2 % of the variation in *Ea*.

## 4. Discussion

It is well known that temperature is a key driver of microbial activity and organic matter decomposition (Alster et al., 2016; Conant et al., 2011; Davidson and Janssens, 2006; Karhu et al., 2014), yet the strength of this temperature response often varies over space due to site-specific soil characteristics at a landscape scale. In our incubation experiment, we observed a consistent increase in PSR rate with rising temperatures, while the magnitude of the response varied depending on the slope positions and soil depths (Fig. 7, Fig. S2). We interpret this spatial heterogeneity as a reflection of field legacy effects, that is, the inherent soil properties (e.g., SOM biogeochemical composition, C/N ratio, and pH) shaped by long-term topographic, hydrological, and thermal interactions across the hillslope.

### 4.1. Topography-induced environmental gradients across the landscape

In our study site, soil temperature, soil VWC, and water table showed great spatial heterogeneity across the hillslope (Fig. 2), reflecting the

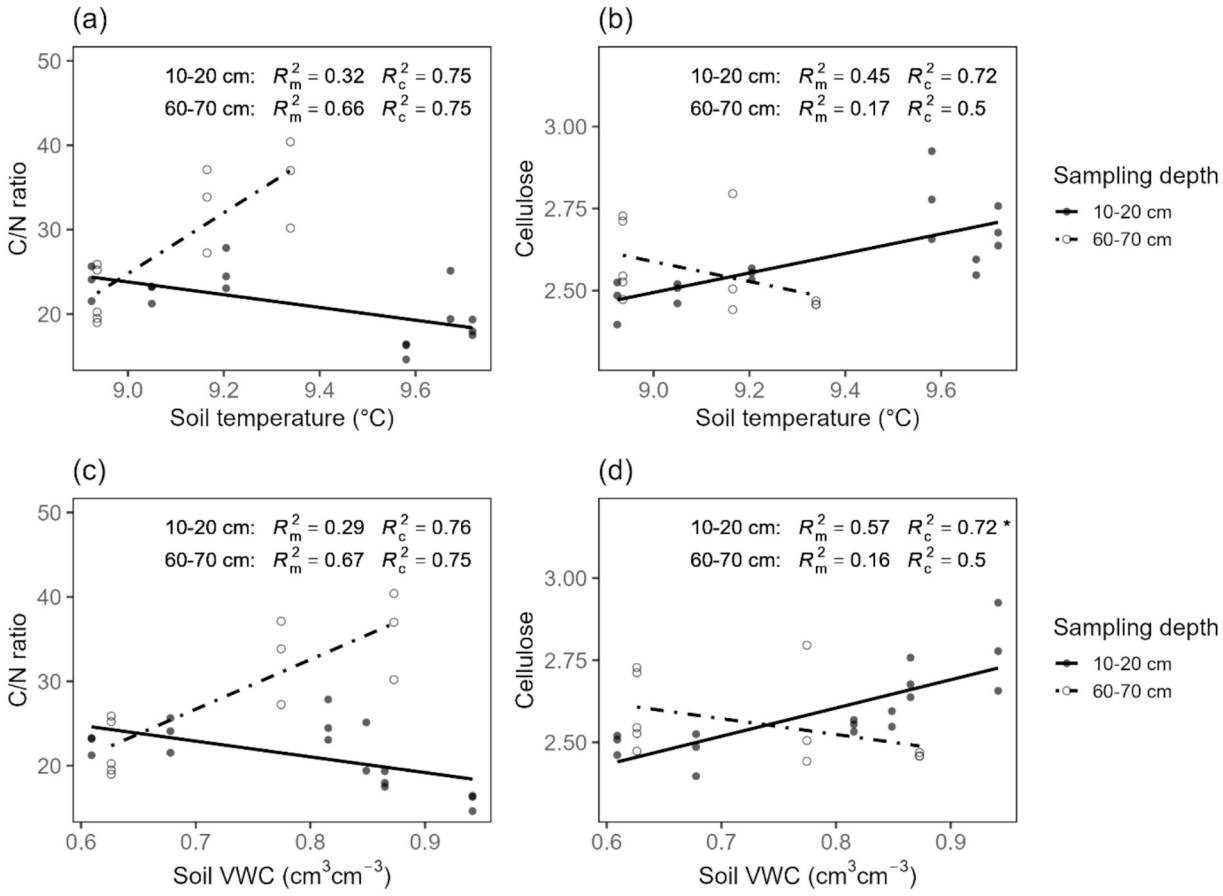


**Fig. 6.** Relationships between C/N ratio and (a) soil temperature, (c) soil VWC, and between the relative abundance of cellulose and (b) soil temperature, (d) soil VWC. Mixed-effects linear regression models were fitted separately for the 10–20 cm and 60–70 cm soil layers, with slope position included as a random effect. The legend reports marginal $R^2$ (*Rm*) and conditional $R^2$ (*Rc*) for each model. Significance level: *** $p < 0.001$, ** $p < 0.01$, * $p < 0.05$.

topographically controlled differences in solar exposure, water flow and accumulation, microclimate, and drainage trajectories. These topographical and thermal-hydrological conditions strongly influenced spatial variability in soil C/N ratio, pH, and SOM biogeochemical composition (Fig. 4a, Fig. 5, and Fig. 6). For instance, hillslope topography act as a first order control by structuring water, nutrients, and energy distribution along the hillslope (Harris and Baird, 2019; Li et al., 2024; Winter, 1988). These gradients determine vegetation composition and productivity, which governs the quantity and quality of organic matter input to the peat soil (Glatzel et al., 2024; Leroy et al., 2017). In turn, these topographically mediated thermal-hydrological conditions influence soil pH and C/N ratio (Fig. S1), which contribute to the selective preservation of SOM and help explain the spatial variation in PSR (Loiko et al., 2019; Philben et al., 2020). Building on this framework, we next explore how these topographic effects are expressed in soil C/N ratio, pH, and SOM composition.

#### 4.1.1. Soil C/N ratio and pH

The spatial variability in C/N ratios reflects how topography regulates both vegetation dynamics and hydrological pathways (Fig. 4a, Fig. 5, Fig. 6). The historically dominant vegetation communities at different slope positions influenced carbon input and N variability due to their interaction with $N_2$-fixing microorganisms (e.g., moss-associated cyanobacteria) (Larmola et al., 2014; Limpens et al., 2006). In addition, potential downslope transport of dissolved organic matter from upper slope positions through surface or subsurface flow may contribute to relatively greater nitrogen accumulation at lower slope positions (e.g., shoulder, Table 2). Consequently, the combination of low N content and elevated recalcitrant carbon in topslope and summit surface peat yields high C/N ratios.

In peatlands, pH is regulated by multiple factors, such as porewater chemistry (Wang et al., 2023), vegetation type (Rydin et al., 2006) and hydrological regimes (Shotyk, 1988), which collectively drive spatial variability in pH across slope positions and depths (see Table 2, Fig. 4a). For instance, the relatively low topsoil pH at the footslope and backslope likely reflects historical dominance by *Sphagnum moss*. As indicated by previous studies, *Sphagnum* actively acidifies its environment through the release of protons ($H^+$) from uronic acids in its cell-wall polymers (e.g., *sphagnan*), while its decomposed residues generate humic acids that further suppress pH (Fissore et al., 2019; Pipes and Yavitt, 2022; Rydin et al., 2006).

#### 4.1.2. SOM biogeochemical composition

At the topslope position, we observed an accumulation of carboxylate, aliphatic, and phenolic functional groups in the upper peat layer (Fig. 3), which can be partly attributed to the dominance of dwarf shrubs (i.e., *Vaccinium myrtillus*) that thrive under relatively dry conditions and supply decay-resistant litter inputs (Bragazza et al., 2013; Wang et al., 2015). In addition, the larger annual water-table fluctuations at the topslope (−21.63 ± 25.17 cm, Fig. 2c) may enhance losses of labile organic components from the shallow peat. Previous studies have shown that large water-table oscillations stimulate microbial oxidation of organic matter (Kim et al., 2021; Rezanezhad et al., 2014), leading to the preferential consumption of easily decomposable materials in the transition zone (Rezanezhad et al., 2014). In contrast, the footslope and backslope positions are characterized by relatively stable water table depths (footslope, −27.11 ± 8.31 cm; backslope, −21.02 ± 7.52 cm), higher VWC, and warmer soil temperature (Fig. 2). These conditions

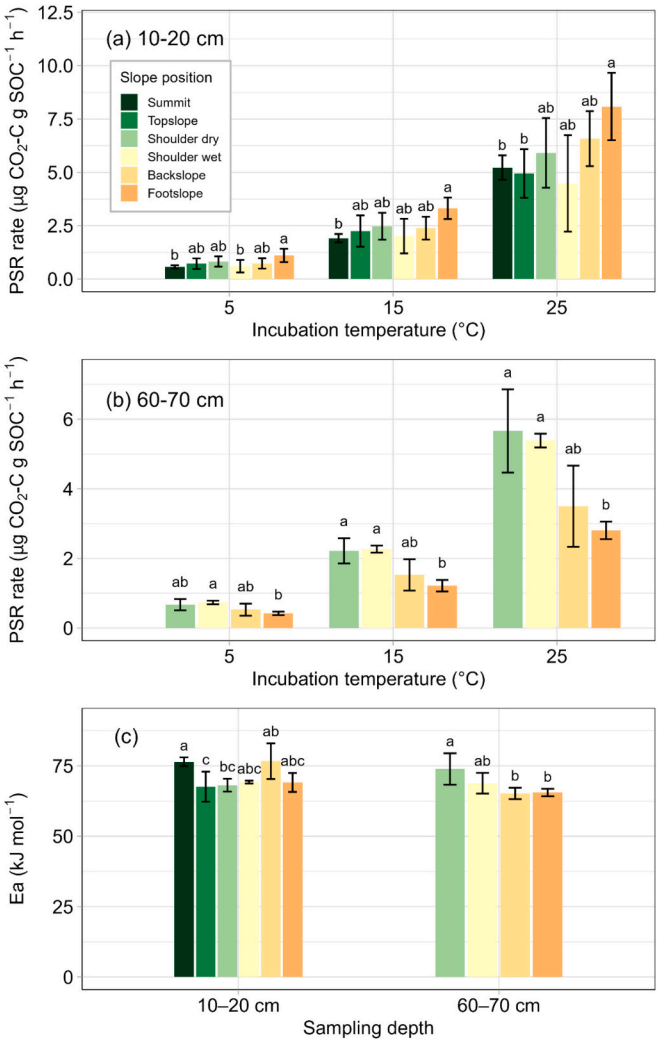


**Fig. 7.** The potential soil respiration (PSR) rate (μg $CO_2$-C g $SOC^{-1}$ $h^{-1}$) across different slope positions and incubation temperature treatments at 10–20 cm depth (a) and 60–70 cm depth (b). The activation energy (*Ea*, KJ $mol^{-1}$) of potential peat soil respiration (c). The error bar indicates one standard deviation. The *Kruskal-Wallis* and *Dunn's test* was conducted to determine if there were significant differences among slope positions, with different letters indicating significant differences.

have been shown to facilitate the establishment and growth of *Sphagnum* moss (Kim et al., 2021; Robroek et al., 2007), which contributes organic matter rich in relatively labile compounds such as cellulose (Heller et al., 2015; Jayasekara et al., 2025; Pipes and Yavitt, 2022). We therefore hypothesize that the historical *Sphagnum* cover might be the primary contributor to the upper peat layers at these areas, as evidenced by macroscopic examination of the peat samples and the relatively high abundance of cellulose. In the field, the high soil moisture, limited oxygen, low pH conditions, and maybe biochemical protection (e.g., structural biopolymers that shield polysaccharides (Pipes and Yavitt, 2022)) might slow down microbial activity, allowing labile substrates to accumulate.

Consistent with observations in peatlands of other regions (Artz et al., 2008; Heller et al., 2015; Hermans et al., 2019; Normand et al., 2017; Tfaily et al., 2014; Webster et al., 2014), we found a higher relative abundance of more recalcitrant compounds and a lower proportion of cellulose in deep layers (i.e., 60–70 cm) compared to the corresponding upper peat layer at most slope positions (Fig. S1). This is because the deep layer receives less input of fresh carbon from aboveground vegetation and remains in a cooler, saturated, and more stable anoxic or semi-anoxic state over long timescales, slowing down the microbial decomposition of organic material (Estop-Aragonés et al., 2022; Rajakaruna et al., 2024; Webster et al., 2014). Under such conditions, labile components may be preferentially decomposed or consumed entirely before reaching deep layers, resulting in a relatively higher proportion of recalcitrant substrates. While at the deep layer of the shoulder slope position, we observed a higher relative abundance of labile components (Fig. 3, Fig. S1). We speculate that during the early stages of peat accumulation, this slope position supported the growth of cellulose-rich vegetation such as *Sphagnum* moss and herbaceous plants. The gentle slope and a high-water table (near the surface) promoted in-situ preservation of these labile inputs under anoxic conditions. Meanwhile, the deep layer likely received soluble organic carbon via vertical leaching from the surface (Rappoldt et al., 2003) and lateral runoff from upslope areas (i.e., topslope and summit) (Glatzel et al., 2024; Holden, 2005; Loiko et al., 2019; Wang et al., 2023).

### 4.2. Spatial variability of potential soil respiration across the landscape

#### 4.2.1. Potential soil respiration rate

It has been reported that the peat biogeochemical composition, particularly the presence of recalcitrant compounds and labile compounds, plays a crucial role in determining the rate of potential soil respiration (Leifeld et al., 2012; Leifeld and von Lützow, 2014; Normand et al., 2021; Webster et al., 2014). In this study, a multiple linear regression analysis revealed that SOM biogeochemical composition was the most important factor in controlling potential soil respiration rates (Table 3). Peat organic matter components directly influence substrate

**Table 3**
Coefficients of multiple linear regression models and relative contributions (in the bracket) of the rotated components (RCs), represented by three types of input variables (i.e., SOM biogeochemical composition, pH, C/N ratio, and thermal-hydrological conditions, see Table S2). These models were used for predicting 1) PSR rates at different incubation temperature conditions and 2) activation energy (*Ea*). Model fit was evaluated using $R^2$ and *RMSE*.

| Input variables | | | Response: PSR rate | | | Response: *Ea* |
|---|---|---|---|---|---|---|
| Variable type | Input | Represented by | 5 °C | 15 °C | 25 °C | |
| SOM biogeochemical composition | RC1: | aliphatic (2858 $cm^{-1}$ and 2926 $cm^{-1}$) and lignin backbone | −0.04 (3 %) | −0.21* (9 %) | −0.54* (9 %) | −1.88* (13 %) |
| | RC2: | cellulose and carboxylic acids | −0.13** (29 %) | −0.36** (27 %) | −1.01*** (31 %) | −0.19 (< 1 %) |
| | RC3: | phenolic (1382 $cm^{-1}$ and 1458 $cm^{-1}$) and carboxylate | −0.01 (< 1 %) | −0.06 (< 1 %) | −0.22 (1 %) | −0.85 (3 %) |
| Other soil biogeochemistry | RC4: | C/N ratio and pH | −0.09* (13 %) | −0.31** (20 %) | −0.93*** (26 %) | −2.22* (18 %) |
| Thermal-hydrological conditions | RC5: | Soil VWC and temp. | −0.01 (< 1 %) | −0.01 (< 1 %) | 0.09 (< 1 %) | 0.80 (2 %) |
| Model performance | $R^2$ | | 0.45 | 0.57 | 0.68 | 0.36 |
| | *RMSE* | | 0.18 | 0.45 | 0.99 | 4.08 |

Significance level: *** $p < 0.001$, ** $p < 0.01$, * $p < 0.05$.

availability (Leifeld et al., 2012), and therefore, spatial variation in these components can lead to the heterogeneity of soil heterotrophic respiration across the landscape (Treat et al., 2015). In the topsoil (i.e., 10–20 cm) at the footslope and backslope positions, higher relative abundances of FTIR signals associated with labile compounds (e.g., cellulose-like carbohydrates) and lower abundances of signals linked to more recalcitrant groups (e.g., phenolics, carboxylate, carboxylic acids, lignin-like, and aliphatic structures) suggest a biogeochemical composition that favors relatively rapid SOC decomposition under drier, aerobic laboratory conditions (Figs. 3, 7a). In contrast, organic matter at other slope positions (e.g., topslope) is characterized by a higher proportion of more recalcitrant components (e.g., aliphatic, Fig. 3), which is associated with slower PSR rates (Fig. 7a). We can therefore infer that, if drying or water-table drawdown occurs due to drought, warming, or drainage, the upper peat layers at the footslope and backslope may become future hotspots of carbon emissions. In this context, peatland rewetting could be an effective climate mitigation strategy, as maintaining wetter conditions could suppress peat respiration and reduce potential carbon losses in a warming world (Holden, 2005). By contrast, SOC stocks at the topslope may remain stable or even increase with dwarf shrubs' expansion (Wang et al., 2015).

Vertical SOM biogeochemical differences (Fig. 3, Fig. S1) also help to explain, in part, the contrasting PSR rates between surface and deeper layers (Fig. 7b). For example, at the shoulder slope position, deep-soil heterotrophic respiration rates exceed those at other slope positions, and in the wetter areas even surpass corresponding topsoil respiration (Fig. 7a, b). The high PSR rates of deep peat can be related to the relatively good substrate quality of deeper layers (Fig. 3a, Hermans et al. (2019)). Although such labile organic materials are preserved in the field under anoxia, our experiments demonstrate that they decompose rapidly once oxygen becomes available (Fig. 7b). This indicates that the deep peat at the shoulder slope position might be another latent $CO_2$ emission hotspot under conditions of warming and water-table drawdown. These findings highlight the vulnerability of peat carbon stocks under future climate scenarios, especially in regions where hydrological regimes are already being altered (Fenner and Freeman, 2011; van Giersbergen et al., 2024).

The C/N ratio is an important factor in explaining spatial heterogeneity in PSR (Fig. 4c, Table 3). On the one hand, the C/N ratio serves as a proxy of organic matter quality, with a lower C/N ratio indicating substrate with more labile components (Bonanomi et al., 2013; Krüger et al., 2015; Taylor et al., 1989). In our study, C/N ratio correlated positively with recalcitrant functional groups (e.g., carboxylic acids; $r = 0.64$; aliphatic at 2926 $cm^{-1}$, $r = 0.55$) and negatively with labile components (e.g., cellulose; $r = -0.49$) (Table S1), in agreement with the findings of other peatlands (Heller et al., 2015; Normand et al., 2017; Webster et al., 2014). This suggests that low C/N soils supply microbes with more accessible carbon and thus exhibit higher potential soil respiration rates. On the other hand, a high C/N ratio implies relative nitrogen limitation for microbial metabolism, thereby slowing biological and ecological processes related to SOC decomposition (Shi et al., 2021; Webster et al., 2014). In our study, topsoil C/N ratios are generally lower than those of deep peat, and topsoil at the footslope and backslope positions exhibit lower C/N than other slope positions (Table 1), which corresponds with the higher PSR rates observed at those depths and locations (Fig. 7a, b).

In the peatland ecosystem, low oxygen availability and acidic conditions impose an “enzymic latch” that inhibits extracellular enzyme activity (Freeman et al., 2001) and reduce bacterial diversity (Rousk et al., 2010). Together, these processes protect the SOC from microbial decomposition in the field. In contrast, higher pH relieves acid inhibition of phenol oxidase and hydrolases and accelerates dissolved organic carbon loss (Kang et al., 2018). However, as labile carbon degrades more rapidly than recalcitrant carbon, this leads to a higher relative proportion of recalcitrant material remaining in-situ and may support a more pH-tolerant functionally diverse microbial community. Consistent with this mechanism, we observed positive correlations between pH and the remaining recalcitrant SOM functional groups (e.g., aliphatic at 2926 $cm^{-1}$; $r = 0.64$, $p < 0.001$) and negative correlations with labile components (e.g., cellulose; $r = -0.42$, $p < 0.05$) (Table S1). When these field legacies were incubated in laboratory conditions, lower-than-average pH samples thus showed higher PSR rates due to higher content of labile materials (e.g., topsoil at backslope position, Fig. 7a).

The long-term thermal-hydrological conditions showed weak correlations with potential soil respiration rates (PSR, Fig. 4c) and contributed little (less than 1 %) to their spatial variability (Table 3). This outcome reflects our experiment design. The PSR rate was measured under a constant soil moisture level (VWC = 0.7 $cm^3\ cm^{-3}$) to isolate the effect of temperature (5, 15, and 25 °C). As a result, the incubation assays reflect PSR under standardized aerobic conditions, with very limited representation of the direct effects of field hydrological conditions on the measured PSR. Their influence in our models, therefore, reflects long-term effects on soil biogeochemistry rather than immediate biogeochemical responses.

#### 4.2.2. *Apparent temperature sensitivity*

Our results indicate that the apparent temperature sensitivity (i.e., *Ea*) of peat potential soil respiration along the hillslope is partially influenced by SOM biogeochemical composition, particularly those more represented by the aliphatic and lignin components (i.e., RC1, Table S2), which explains 13 % of the spatial variance in *Ea* (Table 3). The labile functional groups (e.g., cellulose) exhibit a weaker relationship with *Ea* (Fig. 4c). This likely occurs because these components need less energy to be decomposed, thereby being less sensitive to temperature change (Leifeld et al., 2012; Normand et al., 2021). Some studies have shown that peat substrates with more resistant SOC fractions tend to exhibit higher temperature sensitivity due to higher energy requirements for decomposing complex compounds (Conant et al., 2008; Leifeld and Fuhrer, 2005; Meyer et al., 2018), while others found negative correlations between temperature sensitivity and recalcitrant functional groups, likely due to the physical protection or mineral association of peat SOM that might reduce the substrate availability and accessibility (Moinet et al., 2020; Su et al., 2022; Updegraff et al., 1995). Our results align with the latter findings, showing *Ea* decreased with increasing abundance of recalcitrant functional groups (Table 3, Fig. 4c). For example, the aliphatic structures (i.e., indicative of fats and waxes) are correlated with apparent temperature sensitivity, with Pearson's r values of −0.45 and − 0.48, respectively. This is because those long aliphatic chains are hydrophobic, which limits their interactions with water and extracellular enzymes, resulting in slower decomposition rates and potentially lower apparent temperature sensitivity under our incubation conditions (Goebel et al., 2011; Jiménez-Morillo et al., 2016). Existing studies have demonstrated that the addition of labile substrates enhances soil respiration responses to temperature, resulting in higher apparent temperature sensitivity compared to untreated controls (Weedon et al., 2013; Zhu and Cheng, 2011). Consequently, the higher content of long aliphatic chains and lignin-derived functional groups in deep peat at the footslope and backslope positions helps explain their comparatively low apparent *Ea* values (Fig. 7c).

The soil C/N ratio and pH together could explain 18 % of spatial variability in apparent temperature sensitivity (Table 3, Table S2). This might be partially because the C/N ratio and pH can reveal SOM biogeochemical composition, as discussed in Section 4.2.1. Beyond direct substrate effects, the C/N ratio further regulates apparent temperature sensitivity through microbial community composition and function (Briones et al., 2014; Liu et al., 2021; Xu et al., 2022). In a comprehensive synthesis study that compiled 87 peatland sites across different climate zones, Liu et al. (2024) identified the C/N ratio as one of the primary variables explaining the spatial variations in temperature sensitivity of peat respiration. In addition, numerous studies have established pH regulation of extracellular enzyme activity and microbial

community structure (Freeman et al., 2001; Leifeld and von Lützow, 2014; Preston et al., 2012; Rousk et al., 2010; Xu et al., 2022; Ye et al., 2012). However, it should be noted that the optimal pH varies among different enzymes. For example, Leifeld and von Lützow (2014) found a negative relationship between pH and *Ea* within the pH range of 3.10–5.40. In our study, which covered a similar pH range (3.94–4.95), we also observed a negative correlation between pH and *Ea* (Fig. 4, Table 3). This helps explain why backslope topsoil, with its relatively low pH, displays greater temperature sensitivity (Fig. 7c).

However, a substantial proportion (around 60 %) of the variability in *Ea* remains unexplained by the measured soil biogeochemistry and thermal-hydrological conditions (Table 3). This might be because our incubation experiments were conducted under standardized moisture conditions. Consequently, the analysis cannot capture the direct effects of soil moisture dynamics on *Ea*. Thus, the soil VWC included in the model captures the impact of long-term soil moisture state on soil properties rather than short-term moisture controls, as discussed in section 4.2.1. In addition, we speculate that other factors, such as microbial community composition, likely play an important role. Because different microbial taxa differ in metabolic strategies, enzyme systems, and thermal physiology, leading to distinct temperature sensitivity traits (Alster et al., 2018; Yu et al., 2022). Quantifying their composition and functional traits may increase the explanatory power of *Ea* model and improve the mechanistic understanding of peat decomposition temperature sensitivity.

## 5. Conclusion

Sloping landscapes provide a natural laboratory for understanding how topography-induced environmental gradients interact to shape the spatial variability of potential soil respiration (PSR). In this study, we investigated PSR across a temperate peatland hillslope in the Belgian Hautes Fagnes using controlled laboratory incubation experiments. Our key findings are as follows:

(1) Soil biogeochemistry (i.e., soil pH, C/N ratio, soil organic matter (SOM) functional groups), PSR rates, and apparent temperature sensitivity (i.e., activation energy, *Ea*) varied largely across hillslope positions and soil depths. We found that topographical and thermal-hydrological conditions are associated with soil biogeochemistry patterns across the landscape.
(2) The spatial heterogeneity in PSR and *Ea* was primarily explained by the functional group composition of SOM (45–68 % and 34 % in total, respectively), with cellulose and carboxylic acids accounting for 27 %-31 % of the variation in PSR rates, while aliphatic and lignin functional groups explained 13 % of the variation in *Ea*.
(3) Other soil biogeochemical properties, i.e., C/N ratio and pH, act as the second most important regulators of PSR. They could explain 13 %-26 % of the spatial variability in PSR rates across rising temperatures. Moreover, they play a significant role in regulating potential temperature sensitivity, contributing to 18 % of spatial variance.
(4) The hillslope-governed thermal-hydrological conditions exert cascade effects on PSR. While their direct contribution ($\leq 2$ %) to PSR variation cannot be captured under the standardized incubation conditions, since moisture was held constant, they play a significant indirect role by shaping soil biogeochemical properties in the field.

These results improve our mechanistic understanding of the factors driving potential soil respiration in complex sloping peatland.

## CRediT authorship contribution statement

**Yanfei Li:** Writing – original draft, Visualization, Investigation, Formal analysis, Conceptualization. **Pengzhi Zhao:** Writing – review & editing, Methodology, Conceptualization. **Maud Henrion:** Writing – review & editing, Investigation. **Patrick Gerin:** Writing – review & editing, Resources. **Matthieu Leclercq:** Writing – review & editing, Investigation. **Angus Moore:** Writing – review & editing. **Eléonore du bois d'Aische:** Writing – review & editing. **Sébastien Lambot:** Funding acquisition, Writing – review & editing. **Sophie Opfergelt:** Funding acquisition, Writing – review & editing. **Veerle Vanacker:** Funding acquisition, Writing – review & editing. **François Jonard:** Conceptualization, Funding acquisition, Supervision, Writing – review & editing. **Kristof Van Oost:** Conceptualization, Funding acquisition, Supervision, Writing – review & editing.

## Declaration of competing interest

The authors declare that they have no known competing financial interests or personal relationships that could have appeared to influence the work reported in this paper.

## Acknowledgements

This work is an *Action de Recherche Concertée*, n° 21/26–119, funded by the *Communauté française de Belgique*. Yanfei Li wishes to thank the joint grant from the China Scholarship Council and UCLouvain (No. 202106380030). Kristof *V*an Oost, Sophie Opfergelt, and Sébastien Lambot are supported by the *Fonds de la Recherche Scientifique* (FNRS). The authors would like to thank the *Département de la Nature et des Forêts* (DNF) and Joël Verdin for giving access to the study site. The authors appreciate Thomas Nicolay for his assistance with incubation laboratory work.

## Appendix A. Supplementary data

Supplementary data to this article can be found online at https://doi.org/10.1016/j.catena.2025.109769.

## Data availability

Original data are available on *FigShare*: https://figshare.com/s/79a4c5734d66f5b4336d.

## References

Alster, C.J., Koyama, A., Johnson, N.G., Wallenstein, M.D., von Fischer, J.C., 2016. Temperature sensitivity of soil microbial communities: an application of macromolecular rate theory to microbial respiration. J. Geophys. Res. Biogeo. 121, 1420–1433. https://doi.org/10.1002/2016JG003343.

Alster, C.J., Weller, Z.D., von Fischer, J.C., 2018. A meta-analysis of temperature sensitivity as a microbial trait. Glob. Chang. Biol. 24, 4211–4224. https://doi.org/10.1111/gcb.14342.

Andersen, R., Poulin, M., Borcard, D., Laiho, R., Laine, J., Vasander, H., Tuittila, E.T., 2011. Environmental control and spatial structures in peatland vegetation. J. Veg. Sci. 22, 878–890. https://doi.org/10.1111/j.1654-1103.2011.01295.x.

Artz, R.R.E., Chapman, S.J., Jean Robertson, A.H., Potts, J.M., Laggoun-Défarge, F., Gogo, S., Comont, L., Disnar, J.-R., Francez, A.-J., 2008. FTIR spectroscopy can be used as a screening tool for organic matter quality in regenerating cutover peatlands. Soil Biol. Biochem. 40, 515–527. https://doi.org/10.1016/j.soilbio.2007.09.019.

Becker, T., Kutzbach, L., Forbrich, I., Schneider, J., Jager, D., Thees, B., Wilmking, M., 2008. Do we miss the hot spots? – the use of very high resolution aerial photographs to quantify carbon fluxes in peatlands. Biogeosciences 5, 1387–1393. https://doi.org/10.5194/bg-5-1387-2008.

Berglund, Ö., Berglund, K., 2011. Influence of water table level and soil properties on emissions of greenhouse gases from cultivated peat soil. Soil Biol. Biochem. 43, 923–931. https://doi.org/10.1016/j.soilbio.2011.01.002.

Birnbaum, C., Wood, J., Lilleskov, E., Lamit, L.J., Shannon, J., Brewer, M., Grover, S., 2023. Degradation reduces microbial richness and alters microbial functions in an Australian peatland. Microb. Ecol. 85, 875–891. https://doi.org/10.1007/s00248-022-02071-z.

Bonanomi, G., Incerti, G., Giannino, F., Mingo, A., Lanzotti, V., Mazzoleni, S., 2013. Litter quality assessed by solid state 13C NMR spectroscopy predicts decay rate better than C/N and lignin/N ratios. Soil Biol. Biochem. 56, 40–48. https://doi.org/10.1016/j.soilbio.2012.03.003.

Boothroyd, I.M., Worrall, F., Allott, T.E.H., 2015. Variations in dissolved organic carbon concentrations across peatland hillslopes. J. Hydrol. 530, 372–383. https://doi.org/10.1016/j.jhydrol.2015.10.002.
Bragazza, L., Parisod, J., Buttler, A., Bardgett, R.D., 2013. Biogeochemical plant–soil microbe feedback in response to climate warming in peatlands. Nat. Clim. Change 3, 273–277. https://doi.org/10.1038/nclimate1781.
Briones, M.J.I., McNamara, N.P., Poskitt, J., Crow, S.E., Ostle, N.J., 2014. Interactive biotic and abiotic regulators of soil carbon cycling: evidence from controlled climate experiments on peatland and boreal soils. Glob. Chang. Biol. 20, 2971–2982. https://doi.org/10.1111/gcb.12585.
Burt, T.P., Pinay, G., 2005. Linking hydrology and biogeochemistry in complex landscapes. Prog. Phys. Geogr. 29, 297–316. https://doi.org/10.1191/0309133305pp450ra.
Conant, R.T., Drijber, R.A., Haddix, M.L., Parton, W.J., Paul, E.A., Plante, A.F., Six, J., Steinweg, J.M., 2008. Sensitivity of organic matter decomposition to warming varies with its quality. Glob. Chang. Biol. 14, 868–877. https://doi.org/10.1111/j.1365-2486.2008.01541.x.
Conant, R.T., Ryan, M.G., Ågren, G.I., Birge, H.E., Davidson, E.A., Eliasson, P.E., Evans, S.E., Frey, S.D., Giardina, C.P., Hopkins, F.M., Hyvönen, R., Kirschbaum, M.U. F., Lavallee, J.M., Leifeld, J., Parton, W.J., Megan Steinweg, J., Wallenstein, M.D., Martin Wetterstedt, J.Å., Bradford, M.A., 2011. Temperature and soil organic matter decomposition rates – synthesis of current knowledge and a way forward. Glob. Chang. Biol. 17, 3392–3404. https://doi.org/10.1111/j.1365-2486.2011.02496.x.
Davidson, E.A., Janssens, I.A., 2006. Temperature sensitivity of soil carbon decomposition and feedbacks to climate change. Nature 440, 165–173. https://doi.org/10.1038/nature04514.
Dettmann, U., Kraft, N.N., Rech, R., Heidkamp, A., Tiemeyer, B., 2021. Analysis of peat soil organic carbon, total nitrogen, soil water content and basal respiration: is there a 'best' drying temperature? Geoderma 403, 115231. https://doi.org/10.1016/j.geoderma.2021.115231.
Dioumaeva, I., Trumbore, S., Schuur, E.A.G., Goulden, M.L., Litvak, M., Hirsch, A.I., 2002. Decomposition of peat from upland boreal forest: temperature dependence and sources of respired carbon. J. Geophys. Res. Atmos. 107. https://doi.org/10.1029/2001JD000848. WFX 3-1-WFX 3-12.
Doetterl, S., Six, J., Van Wesemael, B., Van Oost, K., 2012. Carbon cycling in eroding landscapes: geomorphic controls on soil organic C pool composition and C stabilization. Glob. Chang. Biol. 18, 2218–2232. https://doi.org/10.1111/j.1365-2486.2012.02680.x.
Dorrepaal, E., Toet, S., van Logtestijn, R.S.P., Swart, E., van de Weg, M.J., Callaghan, T. V., Aerts, R., 2009. Carbon respiration from subsurface peat accelerated by climate warming in the subarctic. Nature 460, 616–619. https://doi.org/10.1038/nature08216.
Dunn, O.J., 1964. Multiple comparisons using rank sums. Technometrics 6, 241–252. https://doi.org/10.2307/1266041.
Elberling, B., Michelsen, A., Schädel, C., Schuur, E.A.G., Christiansen, H.H., Berg, L., Tamstorf, M.P., Sigsgaard, C., 2013. Long-term CO2 production following permafrost thaw. Nat. Clim. Change 3, 890–894. https://doi.org/10.1038/nclimate1955.
Estop-Aragonés, C., Heffernan, L., Knorr, K.-H., Olefeldt, D., 2022. Limited potential for mineralization of permafrost peatland soil carbon following Thermokarst: evidence from anoxic incubation and priming experiments. Journal of geophysical research. Biogeosciences 127. https://doi.org/10.1029/2022JG006910 e2022JG006910.
Fenner, N., Freeman, C., 2011. Drought-induced carbon loss in peatlands. Nat. Geosci. 4, 895–900. https://doi.org/10.1038/ngeo1323.
Fissore, C., Nater, E.A., McFarlane, K.J., Klein, A.S., 2019. Decadal carbon decomposition dynamics in three peatlands in northern Minnesota. Biogeochemistry 145, 63–79. https://doi.org/10.1007/s10533-019-00591-4.
Fox, J., Monette, G., 1992. Generalized collinearity diagnostics. J. Am. Stat. Assoc. 87, 178–183. https://doi.org/10.2307/2290467.
Frankard, P., Ghiette, P., Hindryckx, M.-N., Schumacker, R., Wastiaux, C., 1998. Peatlands of Wallony (S-Belgium). SUO 49, 33–37.
Freeman, C., Ostle, N., Kang, H., 2001. An enzymic 'latch' on a global carbon store. Nature 409, 149. https://doi.org/10.1038/35051650.
van Giersbergen, Q., Barthelmes, A., Couwenberg, J., Fritz, C., Lång, K., Martin, N., Tanneberger, F., 2024. Identifying hotspots of greenhouse gas emissions from drained peatlands in the European Union. Research Square [preprint]. https://doi.org/10.21203/rs.3.rs-4629642/v1.
Glatzel, S., Worrall, F., Boothroyd, I.M., Heckman, K., 2024. Comparison of the transformation of organic matter flux through a raised bog and a blanket bog. Biogeochemistry 167, 443–459. https://doi.org/10.1007/s10533-023-01093-0.
Goebel, M.-O., Bachmann, J., Reichstein, M., Janssens, I.A., Guggenberger, G., 2011. Soil water repellency and its implications for organic matter decomposition – is there a link to extreme climatic events? Glob. Chang. Biol. 17, 2640–2656. https://doi.org/10.1111/j.1365-2486.2011.02414.x.
Goemaere, E., Demarque, S., Dreesen, R., Declercq, P.-Y.J.G., 2016. The geological and cultural heritage of the Caledonian Stavelot-Venn massif, Belgium. Geoheritage 8, 211–233. https://doi.org/10.1007/s12371-015-0155-y.
Grice, J., 2001. Computing and evaluating factor scores. Psychol. Methods 6, 430–450. https://doi.org/10.1037/1082-989X.6.4.430.
Groemping, U., 2006. Relative importance for linear regression in R: the package relaimpo. J. Stat. Softw. 17, 1–27. https://doi.org/10.18637/jss.v017.i01.
Harris, A., Baird, A.J., 2019. Microtopographic drivers of vegetation patterning in blanket peatlands recovering from Erosion. Ecosystems 22, 1035–1054. https://doi.org/10.1007/s10021-018-0321-6.
Heller, C., Ellerbrock, R.H., Roßkopf, N., Klingenfuß, C., Zeitz, J., 2015. Soil organic matter characterization of temperate peatland soil with FTIR-spectroscopy: effects of mire type and drainage intensity. Eur. J. Soil Sci. 66, 847–858. https://doi.org/10.1111/ejss.12279.
Henrion, M., Li, Y., Koganti, T., Bechtold, M., Jonard, F., Opfergelt, S., Vanacker, V., Van Oost, K., Lambot, S., 2024. Mapping and monitoring peatlands in the Belgian Hautes Fagnes: insights from ground-penetrating radar and electromagnetic induction characterization. Geoderma Reg. 37, e00795. https://doi.org/10.1016/j.geodrs.2024.e00795.
Henrion, M., Li, Y., Wu, K., Jonard, F., Opfergelt, S., Vanacker, V., Van Oost, K., Lambot, S., 2025. Drone-borne ground-penetrating radar reveals spatiotemporal moisture dynamics in peatland root zones. Sci. Remote Sens. 100311. https://doi.org/10.1016/j.srs.2025.100311.
Henry, G.B.L., Awedem Wobiwo, F., Isenborghs, A., Nicolay, T., Godin, B., Stenuit, B.A., Gerin, P.A., 2023. A specific H2/CO2 consumption molar ratio of 3 as a signature for the chain elongation of carboxylates from brewer's spent grain acidogenesis. Front. Bioeng. Biotechnol., Volume 11–2023.
Hermans, R., Zahn, N., Andersen, R., Teh, Y.A., Cowie, N., Subke, J.-A., 2019. An incubation study of GHG flux responses to a changing water table linked to biochemical parameters across a peatland restoration chronosequence. Mires Peat 23, 1–18.
Holden, J., 2005. Peatland hydrology and carbon release: why small-scale process matters. Philos. Trans. R. Soc. A Math. Phys. Eng. Sci. 363, 2891–2913. https://doi.org/10.1098/rsta.2005.1671.
Holden, J., 2009. Topographic controls upon soil macropore flow. Earth Surf. Process. Landf. 34, 345–351. https://doi.org/10.1002/esp.1726.
Hopple, A.M., Wilson, R.M., Kolton, M., Zalman, C.A., Chanton, J.P., Kostka, J., Hanson, P.J., Keller, J.K., Bridgham, S.D., 2020. Massive peatland carbon banks vulnerable to rising temperatures. Nat. Commun. 11, 2373. https://doi.org/10.1038/s41467-020-16311-8.
Iseas, M.S., Rossi, M.F., Aravena Acuña, M.-C., Pancotto, V.A., 2024. Influence of the microtopography of patagonian peatbogs on the fluxes of greenhouse gasses and dissolved carbon in porewater. Ecohydrol. Hydrobiol. https://doi.org/10.1016/j.ecohyd.2024.01.013.
Jayasekara, C., Leigh, C., Shimeta, J., Silvester, E., Grover, S., 2025. Organic matter decomposition in mountain peatlands: effects of substrate quality and peatland degradation. Plant and Soil 506, 639–654. https://doi.org/10.1007/s11104-024-06725-4.
Jiménez-Morillo, N.T., González-Pérez, J.A., Jordán, A., Zavala, L.M., de la Rosa, J.M., Jiménez-González, M.A., González-Vila, F.J., 2016. Organic matter fractions controlling soil water Repellency in Sandy soils from the Doñana National Park (southwestern Spain). Land Degrad. Dev. 27, 1413–1423. https://doi.org/10.1002/ldr.2314.
Jolliffe, I.T., 2002. Principal components in regression analysis. In: Jolliffe, I.T. (Ed.), Principal Component Analysis. Springer, New York, New York, NY, pp. 167–198.
Kang, H., Kwon, M.J., Kim, S., Lee, S., Jones, T.G., Johncock, A.C., Haraguchi, A., Freeman, C., 2018. Biologically driven DOC release from peatlands during recovery from acidification. Nat. Commun. 9, 3807. https://doi.org/10.1038/s41467-018-06259-1.
Karhu, K., Auffret, M.D., Dungait, J.A.J., Hopkins, D.W., Prosser, J.I., Singh, B.K., Subke, J.-A., Wookey, P.A., Ågren, G.I., Sebastià, M.-T., Gouriveau, F., Bergkvist, G., Meir, P., Nottingham, A.T., Salinas, N., Hartley, I.P., 2014. Temperature sensitivity of soil respiration rates enhanced by microbial community response. Nature 513, 81–84. https://doi.org/10.1038/nature13604.
Keiser, A.D., Davis, C.L., Smith, M., Bell, S.L., Hobbie, E.A., Hofmockel, K.S., 2024. Depth and microtopography influence microbial biogeochemical processes in a forested peatland. Plant and Soil. https://doi.org/10.1007/s11104-024-06895-1.
Kim, J., Rochefort, L., Hogue-Hugron, S., Alqulaiti, Z., Dunn, C., Pouliot, R., Jones, T.G., Freeman, C., Kang, H., 2021. Water table fluctuation in peatlands facilitates fungal proliferation, impedes Sphagnum growth and accelerates decomposition. Front. Earth Sci. 8–2020.
Krüger, J.P., Leifeld, J., Glatzel, S., Szidat, S., Alewell, C., 2015. Biogeochemical indicators of peatland degradation – a case study of a temperate bog in northern Germany. Biogeosciences 12, 2861–2871. https://doi.org/10.5194/bg-12-2861-2015.
Lal, R., Shukla, M.K., 2004. Principles of Soil Physics. CRC Press. https://doi.org/10.4324/9780203021231.
Larmola, T., Leppänen, S.M., Tuittila, E.-S., Aarva, M., Merilä, P., Fritze, H., Tiirola, M., 2014. Methanotrophy induces nitrogen fixation during peatland development. Proc. Natl. Acad. Sci. 111, 734–739. https://doi.org/10.1073/pnas.1314284111.
Leifeld, J., Fuhrer, J., 2005. The temperature response of CO2 production from bulk soils and soil fractions is related to soil organic matter quality. Biogeochemistry 75, 433–453. https://doi.org/10.1007/s10533-005-2237-4.
Leifeld, J., von Lützow, M., 2014. Chemical and microbial activation energies of soil organic matter decomposition. Biol. Fertil. Soils 50, 147–153. https://doi.org/10.1007/s00374-013-0822-6.
Leifeld, J., Steffens, M., Galego-Sala, A., 2012. Sensitivity of peatland carbon loss to organic matter quality. Geophys. Res. Lett. 39, L14704. https://doi.org/10.1029/2012GL051856.
Leroy, F., Gogo, S., Guimbaud, C., Bernard-Jannin, L., Hu, Z., Laggoun-Défarge, F., 2017. Vegetation composition controls temperature sensitivity of CO2 and CH4 emissions and DOC concentration in peatlands. Soil Biol. Biochem. 107, 164–167. https://doi.org/10.1016/j.soilbio.2017.01.005.
Li, C., Grayson, R., Holden, J., Li, P., 2018. Erosion in peatlands: recent research progress and future directions. Earth Sci. Rev. 185, 870–886. https://doi.org/10.1016/j.earscirev.2018.08.005.
Li, Q., Leroy, F., Zocatelli, R., Gogo, S., Jacotot, A., Guimbaud, C., Laggoun-Défarge, F., 2021. Abiotic and biotic drivers of microbial respiration in peat and its sensitivity to

temperature change. Soil Biol. Biochem. 153, 108077. https://doi.org/10.1016/j.soilbio.2020.108077.
Li, Y., Henrion, M., Moore, A., Lambot, S., Opfergelt, S., Vanacker, V., Jonard, F., Van Oost, K., 2024. Factors controlling peat soil thickness and carbon storage in temperate peatlands based on UAV high-resolution remote sensing. Geoderma 449, 117009. https://doi.org/10.1016/j.geoderma.2024.117009.
Li, Y., Henrion, M., Moore, A., Lambot, S., Opfergelt, S., Vanacker, V., Jonard, F., Van Oost, K., 2025. Hot spots, hot moments, and spatiotemporal drivers of soil CO2 flux in temperate peatlands using UAV remote sensing. Biogeosciences 2025, 1–37. https://doi.org/10.5194/egusphere-2025-1595.
Limpens, J., Heijmans, M.M.P.D., Berendse, F., 2006. The nitrogen cycle in boreal peatlands. In: Wieder, R.K., Vitt, D.H. (Eds.), Boreal Peatland Ecosystems. Springer, Berlin Heidelberg, Berlin, Heidelberg, pp. 195–230.
Liu, C., Liu, J., Zhou, C., Huang, X., Wang, H., 2021. Redox potential and C/N ratio predict the structural shift of mercury methylating microbe communities in a subalpine Sphagnum peatland. Geoderma 403, 115375. https://doi.org/10.1016/j.geoderma.2021.115375.
Liu, H., Rezanezhad, F., Zhao, Y., He, H., Van Cappellen, P., Lennartz, B., 2024. The apparent temperature sensitivity (Q10) of peat soil respiration: a synthesis study. Geoderma 443, 116844. https://doi.org/10.1016/j.geoderma.2024.116844.
Loiko, S., Raudina, T., Lim, A., Kuzmina, D., Kulizhskiy, S., Pokrovsky, O., 2019. Microtopography controls of carbon and related elements distribution in the West Siberian frozen bogs. Geosciences 9, 291. https://doi.org/10.3390/geosciences9070291.
Loisel, J., van Bellen, S., Pelletier, L., Talbot, J., Hugelius, G., Karran, D., Yu, Z., Nichols, J., Holmquist, J., 2017. Insights and issues with estimating northern peatland carbon stocks and fluxes since the last glacial maximum. Earth-Sci. Rev. 165, 59–80. https://doi.org/10.1016/j.earscirev.2016.12.001.
Loisel, J., Gallego-Sala, A.V., Amesbury, M.J., Magnan, G., Anshari, G., Beilman, D.W., Benavides, J.C., Blewett, J., Camill, P., Charman, D.J., Chawchai, S., Hedgpeth, A., Kleinen, T., Korhola, A., Large, D., Mansilla, C.A., Müller, J., van Bellen, S., West, J. B., Yu, Z., Bubier, J.L., Garneau, M., Moore, T., Sannel, A.B.K., Page, S., Väliranta, M., Bechtold, M., Brovkin, V., Cole, L.E.S., Chanton, J.P., Christensen, T. R., Davies, M.A., De Vleeschouwer, F., Finkelstein, S.A., Frolking, S., Gałka, M., Gandois, L., Girkin, N., Harris, L.I., Heinemeyer, A., Hoyt, A.M., Jones, M.C., Joos, F., Juutinen, S., Kaiser, K., Lacourse, T., Lamentowicz, M., Larmola, T., Leifeld, J., Lohila, A., Milner, A.M., Minkkinen, K., Moss, P., Naafs, B.D.A., Nichols, J., O'Donnell, J., Payne, R., Philben, M., Piilo, S., Quillet, A., Ratnayake, A. S., Roland, T.P., Sjögersten, S., Sonnentag, O., Swindles, G.T., Swinnen, W., Talbot, J., Treat, C., Valach, A.C., Wu, J., 2021. Expert assessment of future vulnerability of the global peatland carbon sink. Nat. Clim. Change 11, 70–77. https://doi.org/10.1038/s41558-020-00944-0.
Meyer, N., Welp, G., Amelung, W., 2018. The temperature sensitivity (Q10) of soil respiration: controlling factors and spatial prediction at regional scale based on environmental soil classes. Global Biogeochem. Cycles 32, 306–323. https://doi.org/10.1002/2017GB005644.
Millar, D.J., Cooper, D.J., Ronayne, M.J., 2018. Groundwater dynamics in mountain peatlands with contrasting climate, vegetation, and hydrogeological setting. J. Hydrol. 561, 908–917. https://doi.org/10.1016/j.jhydrol.2018.04.050.
Moinet, G.Y.K., Moinet, M., Hunt, J.E., Rumpel, C., Chabbi, A., Millard, P., 2020. Temperature sensitivity of decomposition decreases with increasing soil organic matter stability. Sci. Total Environ. 704, 135460. https://doi.org/10.1016/j.scitotenv.2019.135460.
Moore, T.R., Dalva, M., 1997. Methane and carbon dioxide exchange potentials of peat soils in aerobic and anaerobic laboratory incubations. Soil Biol. Biochem. 29, 1157–1164. https://doi.org/10.1016/S0038-0717(97)00037-0.
Mormal, P., Tricot, C., 2004. Aperçu climatique des Hautes-Fagnes. Institut Royal météorologique de Belgique, Brussel.
Murdoch, D.J., Chow, E.D., 1996. A graphical display of Large correlation matrices. Am. Stat. 50, 178–180. https://doi.org/10.2307/2684435.
Normand, A.E., Smith, A.N., Clark, M.W., Long, J.R., Reddy, K.R., 2017. Chemical composition of soil organic matter in a subarctic peatland: influence of shifting vegetation communities. Soil Sci. Soc. Am. J. 81, 41–49. https://doi.org/10.2136/sssaj2016.05.0148.
Normand, A.E., Turner, B.L., Lamit, L.J., Smith, A.N., Baiser, B., Clark, M.W., Hazlett, C., Kane, E.S., Lilleskov, E., Long, J.R., Grover, S.P., Reddy, K.R., 2021. Organic matter chemistry drives carbon dioxide production of peatlands. Geophys. Res. Lett. 48, e2021GL093392. https://doi.org/10.1029/2021GL093392.
Ofiti, N.O.E., Schmidt, M.W.I., Abiven, S., Hanson, P.J., Iversen, C.M., Wilson, R.M., Kostka, J.E., Wiesenberg, G.L.B., Malhotra, A., 2023. Climate warming and elevated CO2 alter peatland soil carbon sources and stability. Nat. Commun. 14, 7533. https://doi.org/10.1038/s41467-023-43410-z.
Philben, M., Taş, N., Chen, H., Wullschleger, S., Kholodov, A., Graham, D., Gu, B., 2020. Influences of hillslope biogeochemistry on anaerobic soil organic matter decomposition in a tundra watershed. J. Geophys. Res. Biogeo. 125. https://doi.org/10.1029/2019JG005512.
Pipes, G.T., Yavitt, J.B., 2022. Biochemical components of Sphagnum and persistence in peat soil. Can. J. Soil Sci. 102, 785–795. https://doi.org/10.1139/cjss-2021-0137.
Preston, M.D., Basiliko, N., 2016. Carbon mineralization in peatlands: does the soil microbial community composition matter? Geomicrobiol J. 33, 151–162. https://doi.org/10.1080/01490451.2014.999293.
Preston, M.D., Smemo, K.A., McLaughlin, J.W., Basiliko, N., 2012. Peatland microbial communities and decomposition processes in the james bay lowlands, Canada. Front. Microbiol. 3, 70. https://doi.org/10.3389/fmicb.2012.00070.
Rajakaruna, S., Makke, G., Grachet, N.G., Ayala-Ortiz, C., Bouranis, J., Hoyt, D.W., Toyoda, J., Denis, E.H., Moran, J.J., Song, T., Sun, X., Eder, E.K., Wong, A.R., Chu, R., Heyman, H., Kolton, M., Chanton, J.P., Wilson, R.M., Kostka, J., Tfaily, M. M., 2024. Adding labile carbon to peatland soils triggers deep carbon breakdown. Commun. Earth Environ. 5, 792. https://doi.org/10.1038/s43247-024-01954-y.
Rappoldt, C., Pieters, G.-J.J.M., Adema, E.B., Baaijens, G.J., Grootjans, A.P., van Duijn, C. J., 2003. Buoyancy-driven flow in a peat moss layer as a mechanism for solute transport. Proc. Natl. Acad. Sci. 100, 14937–14942. https://doi.org/10.1073/pnas.1936122100.
Revelle, W., 2009. An Introduction to Psychometric Theory with Applications in R. Springer. http://personality-project.org/r/book.
Rezanezhad, F., Couture, R.M., Kovac, R., O'Connell, D., Van Cappellen, P., 2014. Water table fluctuations and soil biogeochemistry: an experimental approach using an automated soil column system. J. Hydrol. 509, 245–256. https://doi.org/10.1016/j.jhydrol.2013.11.036.
Robroek, B., Limpens, J., Breeuwer-Spierings, A., Schouten, M.G.C., 2007. Effects of water level and temperature on performance of four Sphagnum mosses. Plant Ecol. 190, 97–107. https://doi.org/10.1007/s11258-006-9193-5.
Rousk, J., Bååth, E., Brookes, P.C., Lauber, C.L., Lozupone, C., Caporaso, J.G., Knight, R., Fierer, N., 2010. Soil bacterial and fungal communities across a pH gradient in an arable soil. ISME J. 4, 1340–1351. https://doi.org/10.1038/ismej.2010.58.
Rydin, H., Gunnarsson, U., Sundberg, S., 2006. The role of Sphagnum in peatland development and persistence. In: Wieder, R.K., Vitt, D.H. (Eds.), Boreal Peatland Ecosystems. Springer, Berlin Heidelberg, Berlin, Heidelberg, pp. 47–65.
Schuur, E.A.G., McGuire, A.D., Schädel, C., Grosse, G., Harden, J.W., Hayes, D.J., Hugelius, G., Koven, C.D., Kuhry, P., Lawrence, D.M., Natali, S.M., Olefeldt, D., Romanovsky, V.E., Schaefer, K., Turetsky, M.R., Treat, C.C., Vonk, J.E., 2015. Climate change and the permafrost carbon feedback. Nature 520, 171–179. https://doi.org/10.1038/nature14338.
Shi, Y., Zhang, X., Wang, Z., Xu, Z., He, C., Sheng, L., Liu, H., Wang, Z., 2021. Shift in nitrogen transformation in peatland soil by nitrogen inputs. Sci. Total Environ. 764, 142924. https://doi.org/10.1016/j.scitotenv.2020.142924.
Shotyk, W., 1988. Review of the inorganic geochemistry of peats and peatland waters. Earth-Sci. Rev. 25, 95–176. https://doi.org/10.1016/0012-8252(88)90067-0.
Sjögersten, S., Caul, S., Daniell, T.J., Jurd, A.P.S., O'Sullivan, O.S., Stapleton, C.S., Titman, J.J., 2016. Organic matter chemistry controls greenhouse gas emissions from permafrost peatlands. Soil Biol. Biochem. 98, 42–53. https://doi.org/10.1016/j.soilbio.2016.03.016.
Skopp, J.M., 2000. Physical properties of primary particles. in: Huang, P.M., Li, Y., Sumner, M.E. (Eds.), Handbook of Soil Sciences. CRC press, Boca Raton, 3–17.
Sloan, T., Payne, R., Anderson, R., Bain, C., Chapman, S., Cowie, N., Gilbert, P.J., Lindsay, R., Mauquoy, D., Newton, A., Andersen, R., 2018. Peatland afforestation in the UK and consequences for carbon storage. Mires Peat 23, 10.19189/MaP.2017.OMB.315.
Su, J., Zhang, H., Han, X., Peñuelas, J., Filimonenko, E., Jiang, Y., Kuzyakov, Y., Wei, C., 2022. Low carbon availability in paleosols nonlinearly attenuates temperature sensitivity of soil organic matter decomposition. Glob. Chang. Biol. 28, 4180–4193. https://doi.org/10.1111/gcb.16183.
Sullivan, P.F., Arens, S.J.T., Chimner, R.A., Welker, J.M., 2008. Temperature and microtopography interact to control carbon cycling in a high Arctic fen. Ecosystems 11, 61–76. https://doi.org/10.1007/s10021-007-9107-y.
Taylor, B.R., Parkinson, D., William, F.J.P., 1989. Nitrogen and lignin content as predictors of litter decay rates: a microcosm test. Ecology 70, 97–104. https://doi.org/10.2307/1938416.
Tfaily, M.M., Cooper, W.T., Kostka, J.E., Chanton, P.R., Schadt, C.W., Hanson, P.J., Iversen, C.M., Chanton, J.P., 2014. Organic matter transformation in the peat column at Marcell experimental Forest: humification and vertical stratification. J. Geophys. Res. Biogeo. 119, 661–675. https://doi.org/10.1002/2013JG002492.
Treat, C.C., Wollheim, W.M., Varner, R.K., Grandy, A.S., Talbot, J., Frolking, S., 2014. Temperature and peat type control CO2 and CH4 production in Alaskan permafrost peats. Glob. Chang. Biol. 20, 2674–2686. https://doi.org/10.1111/gcb.12572.
Treat, C.C., Natali, S.M., Ernakovich, J., Iversen, C.M., Lupascu, M., McGuire, A.D., Norby, R.J., Roy Chowdhury, T., Richter, A., Šantrůčková, H., Schädel, C., Schuur, E. A.G., Sloan, V.L., Turetsky, M.R., Waldrop, M.P., 2015. A pan-Arctic synthesis of CH4 and CO2 production from anoxic soil incubations. Glob. Chang. Biol. 21, 2787–2803. https://doi.org/10.1111/gcb.12875.
UNEP, 2022. Global Peatlands Assessment – The State of the World's Peatlands: Evidence for Action toward the Conservation, Restoration, and Sustainable Management of Peatlands. 9789280739916, Global Peatlands Initiative, United Nations Environment Programme.
Updegraff, K., Pastor, J., Bridgham, S.D., Johnston, C.A., 1995. Environmental and substrate controls over carbon and nitrogen mineralization in northern wetlands. Ecol. Appl. 5, 151–163. https://doi.org/10.2307/1942060.
Wang, H., Richardson, C.J., Ho, M., 2015. Dual controls on carbon loss during drought in peatlands. Nat. Clim. Chang. 5, 584–587. https://doi.org/10.1038/nclimate2643.
Wang, M., Wang, S., Cao, Y., Jiang, M., Wang, G., Dong, Y., 2021. The effects of hummock-hollow microtopography on soil organic carbon stocks and soil labile organic carbon fractions in a sedge peatland in Changbai Mountain, China. CATENA 201, 105204. https://doi.org/10.1016/j.catena.2021.105204.
Wang, M., Liu, H., Rezanezhad, F., Zak, D., Lennartz, B., 2023. The influence of microtopography on soil carbon accumulation and nutrient release from a rewetted coastal peatland. Geoderma 438, 116637. https://doi.org/10.1016/j.geoderma.2023.116637.
Webster, K.L., Creed, I.F., Malakoff, T., Delaney, K., 2014. Potential vulnerability of deep carbon deposits of forested swamps to drought. Soil Sci. Soc. Am. J. 78, 1097–1107. https://doi.org/10.2136/sssaj2013.10.0436.
Weedon, J.T., Aerts, R., Kowalchuk, G.A., van Logtestijn, R., Andringa, D., van Bodegom, P.M., 2013. Temperature sensitivity of peatland C and N cycling: does

substrate supply play a role? Soil Biol. Biochem. 61, 109–120. https://doi.org/10.1016/j.soilbio.2013.02.019.

Wiaux, F., Vanclooster, M., Cornelis, J.T., Van Oost, K., 2014. Factors controlling soil organic carbon persistence along an eroding hillslope on the loess belt. Soil Biol. Biochem. 77, 187–196. https://doi.org/10.1016/j.soilbio.2014.05.032.

Wickland, K.P., Neff, J.C., 2008. Decomposition of soil organic matter from boreal black spruce forest: environmental and chemical controls. Biogeochemistry 87, 29–47. https://doi.org/10.1007/s10533-007-9166-3.

Widyastuti, M.T., Minasny, B., Padarian, J., Maggi, F., Aitkenhead, M., Beucher, A., Connolly, J., Fiantis, D., Kidd, D., Ma, Y., Macfarlane, F., Robb, C., Rudiyanto, Setiawan, B.I., Taufik, M., 2025. Digital mapping of peat thickness and carbon stock of global peatlands. CATENA, 258, 109243. doi:https://doi.org/10.1016/j.catena.2025.109243.

Winter, T.C., 1988. A conceptual framework for assessing cumulative impacts on the hydrology of nontidal wetlands. Environ. Manag. 12, 605–620. https://doi.org/10.1007/BF01867539.

Xu, Z., Wang, Y., Sun, D., Li, H., Dong, Y., Wang, Z., Wang, S., 2022. Soil nutrients and nutrient ratios influence the ratios of soil microbial biomass and metabolic nutrient limitations in mountain peatlands. CATENA 218, 106528. https://doi.org/10.1016/j.catena.2022.106528.

Ye, R., Jin, Q., Bohannan, B., Keller, J.K., McAllister, S.A., Bridgham, S.D., 2012. pH controls over anaerobic carbon mineralization, the efficiency of methane production, and methanogenic pathways in peatlands across an ombrotrophic–minerotrophic gradient. Soil Biol. Biochem. 54, 36–47. https://doi.org/10.1016/j.soilbio.2012.05.015.

Yu, K., van den Hoogen, J., Wang, Z., Averill, C., Routh, D., Smith, G.R., Drenovsky, R.E., Scow, K.M., Mo, F., Waldrop, M.P., Yang, Y., Tang, W., De Vries, F.T., Bardgett, R.D., Manning, P., Bastida, F., Baer, S.G., Bach, E.M., García, C., Wang, Q., Ma, L., Chen, B., He, X., Teurlincx, S., Heijboer, A., Bradley, J.A., Crowther, T.W., 2022. The biogeography of relative abundance of soil fungi versus bacteria in surface topsoil. Earth Syst. Sci. Data 14, 4339–4350. https://doi.org/10.5194/essd-14-4339-2022.

Zhang, L., Liu, X., Duddleston, K., Hines, M.E., 2020. The effects of pH, temperature, and humic-like substances on anaerobic carbon degradation and methanogenesis in ombrotrophic and Minerotrophic Alaskan peatlands. Aquat. Geochem. 26, 221–244. https://doi.org/10.1007/s10498-020-09372-0.

Zhao, P., Fallu, D., Cucchiaro, S., Waddington, C., Cockcroft, D., Snape, L., Lang, A., Doetterl, S., Brown, T., Oost, K., 2021. Soil organic carbon stabilization mechanisms and temperature sensitivity in old terraced soils. Biogeosciences 18, 6301–6312. https://doi.org/10.5194/bg-18-6301-2021.

Zhu, B., Cheng, W., 2011. Rhizosphere priming effect increases the temperature sensitivity of soil organic matter decomposition. Glob. Chang. Biol. 17, 2172–2183. https://doi.org/10.1111/j.1365-2486.2010.02354.x.